Cascade multi-resonant disturbance observer design. Application to a distillation column*

I. Peñarrocha-Alós[a], D. Tena[a], R. Sanchis[a]

[a] *Departament d'Enginyeria de Sistemes Industrials i Disseny. Universitat Jaume I de Castelló, Spain (e-mail: {ipenarro,david.tenatena,rsanchis}@uji.es).*

Abstract

In this work, we present a novel approach for input disturbance estimation design and implementation for dynamical processes under the influence of unknown disturbances that present a clear periodical behaviour of a known frequency. Both the design and the implementation are focused on simplicity. The observer consists of a set of transfer functions fed by the process manipulated variable and the sensor measurement that are implemented through a mixture of cascade and series connections. For the synthesis of the disturbance observer, we just need an input-output model of the process and one tuning parameter in each of the transfer functions. We present simple rules for the design considering the trade-off between the transient time needed to estimate changes in the behaviour of the disturbance and the robustness against measurement noise effects. We show the benefits in using this disturbance estimation as a feed-forward signal in both open loop and closed loop control applications, and we quantify the robustness modification when used together with a closed loop controller. The transfer functions of the observer include both a low pass filter and a set of resonant terms. We quantify the effect of the different terms and their parameter tuning. Our implementation method uses standard tools available in industrial control systems and we have applied it to a real distillation column under ambient temperature disturbances. The main contribution of this work is the simplicity of the design and implementation of the disturbance observer, making it suitable for the process industry and to be managed by non-experts in control systems. Another contribution is the *a priori* design based in intuitive engineering performance indices.

Keywords: Periodic disturbances, Disturbance Observer (DOB), Multiresonant term

1. Introduction

Many kinds of disturbances usually affect industrial systems, from sensor or actuator malfunctions to environmental conditions or other systems coupling. This fact explains why feedback control is needed: its main task is to ensure that these disturbances do not compromise the system performance and stability [1]. Control of systems under disturbances can be based on passive strategies—where the controller must reject the disturbance without using any information about the disturbance—or active strategies—where the disturbance is measured or estimated and then incorporated into the control action. The PID controller is a good example of the first one. For the second strategy, when disturbance signal is not available, we need to estimate or observe it from the measurable variables and the knowledge of the system. The algorithm used for disturbance estimation is typically referred to as a Disturbance Observer (DOB) [2].

Besides its use in control, disturbance estimation is also useful for other purposes, like fault diagnosis and actuator sizing. In fault diagnosis, the disturbance—also called fault—estimation is combined with a decision mechanism, so that we consider that the system is under a fault if the fault estimation fulfils the condition determined in the decision mechanism [3, 4, 5]. A widespread practice is to use a threshold in a detection mechanism, so if the fault estimation is beyond the threshold, we assume a fault has occurred. Disturbance estimation can be also useful for control actuators sizing. If we can estimate the magnitude of process disturbances, we would know the amount of control action needed from the actuator and this will help us to choose its size. Due to the mentioned relevance of disturbance estimation in several applications, DOB design and application has emerged as an important topic in academic research over the years [6, 7, 8, 9].

In this work we focus on periodic disturbances, which are those expected to occur continuously and cyclically. As we will discuss later, the estimation of these disturbances requires a different approach w.r.t the estimation of faults—sudden or progressive disturbances that only occur in abnormal situations. Previous work on the estimation of periodic disturbances has been done for several applications, like power electronics [10, 11, 12, 13, 14], permanent magnets motors [15], power grids [16, 17, 18], industrial

*This work was supported by the Spanish State Research Agency under grants PID2021-125634OB-I00 and TED2021-130120B-C22, ERDF, EU; and the Universitat Jaume I through project number UJI-B2021-45.

repetitive tasks with robotic arms [19], mechanical systems under vibrations [20, 21, 22, 23] or wind turbines [24].

Many kinds of different disturbance observers have been proposed [2, 25, 26, 27], and particularly for periodic disturbances [28, 29, 30, 31]. State space observers have been used for fault detection [32, 33, 34] and in Active Disturbance Rejection Controllers (ADRC) [35, 36, 37, 38] handling also periodical behaviour.

Other kind of observers are based in an additive structure implemented in input-output transfer functions, whose design consists of inverting the process model to estimate the disturbance. To ensure the observer is proper, they include a filter—called Q-filter—so the relative degree of the inverted plant transfer function plus the filter is not negative. The observed disturbance is commonly feed-forwarded into a feedback controller and can be found in literature as DOB (Disturbance Observer). The design of the Q-filter is critical for the use of DOB for periodic disturbances because the use of a simple low-pass filter—this is the most common filter used in applications of non-periodic disturbances—will lead to out of phase, and thus delayed, estimation of the periodic disturbance.

Several solutions have been presented for DOB under periodic disturbances. Some authors use the combination of a DOB for estimating low frequency components of the disturbances and other solutions for periodic components [29], like an infinite order DOB [39], a periodic DOB suitable for aperiodic disturbances [40], or an adaptive notch filter based in the implementation of a time delay [19]. On [21], a phase-lead compensator is used to ensure phased estimation. On [15], an adaptive mechanism is also used to correct the phase change and magnitude distortion caused by the Q-filter. On [13], a multiplicative approach of several resonant filters is used. On [41], the problem is expanded to the MIMO case and an optimal strategy is used for the estimator tuning, by minimizing H_∞ norm of the disturbance estimation error.

In the context of process industry—such as refining, chemical or oil&gas—, control and estimation tasks are usually programmed in a Distributed Control System (DCS) via so-called Function Blocks, which are pre-configured software components ready to implement standard algorithms like PID controllers, low-pass filters, lead-lag compensators, etc. [42]. These Function Blocks contain encapsulated algorithms ready to work after plugging input and output signals and setting some parameters. This has somehow democratized the use of control algorithms since they have substituted script programming—which may require a deeper knowledge—to block selection and plug&play programming, so far, more people can develop tasks on control configuration, even with less control theory or programming background.

Motivated by this paradigm in the context of process industry, the aim of this work is to design a periodic disturbance observer whose design—in terms of parameters tuning—and implementation are simple and can be implemented through standard tools available in Distributed Control Systems. The objective is to find an additive structure that can be connected or disconnected, and where adjustment is limited to a few parameters' calibration. Moreover, these parameters would ideally have some physical meaning, i.e., they are related to some properties of the process like process gains or times related to dynamics of the process or the estimator. Despite the search of simplicity in the design and implementation, this does not prevent us of being rigorous in the analysis.

To achieve the previous statement, no state-space realization is considered, because this would lead to an implementation with lots of parameters with no physical meaning (specially in high order systems). We base our implementation in continuous transfer functions (assuming a DCS can to discretize them according to the corresponding sampling period) with the lowest possible order (that depends on the system model) to ensure minimum number of tuning parameters for each application. We propose to use a bank of multi-resonant disturbance observers, including one for low frequency component estimation and others so that each one estimates a frequency component. One can add up as many transfer functions as frequencies that are expected to be present in the periodic disturbance, and each of them is implemented in a cascade configuration following the previous ones.

Main contributions of the work are:

- A cascade additive-multiplicative scalable filter structure based on simple transfer functions, that allows the easy implementation in industrial control systems, and that allows the user to easily add terms for the estimation of new frequency components, without affecting the previous ones.

- An uncomplicated design strategy to tune the small number of tuning parameters based on straightforward relationships between those parameters and time response performance and measurement noise effect.

This contributions are considered the advantages of applying our proposal w.r.t. other approaches in the literature as it is shown in the different comparison that are presented.

The proposed estimator has been tested in a real distillation column from a nylon manufacturing factory, which is used to treat a 10t/h stream of cyclohexane oxidation products. This distillation column is affected by periodical disturbances due to the ambient temperature—climate behaves as a 24-hour periodic disturbance, as shown in [43]. We can accurately estimate the disturbance and determine the control action that should be feed-forwarded to cancel it.

The paper is structured as follows. Section 2 presents the problem statement. On section 3, we discuss the disturbance estimator structure, arguing the structure choice and analysing its implications. Section 4 introduces first the estimation error analysis, including the convergence

and high frequency measurement noise attenuation, and addresses the disturbance estimator tuning, including practical rules for the user. In section 5 we analyse the use of this disturbance estimate in control applications as a feedforward signal in both open and closed loop control. In Section 6 we compare our method with other ones present in the literature. Section 7 consists of a numerical example to clarify and illustrate the proposal, and to compare it with other approaches. Section 8 presents a case study of an industrial distillation column, where we apply the proposed disturbance estimator to real historical operating data to estimate the effect of ambient temperature on the column behaviour. Finally, section 9 summarizes the conclusions of the paper.

2. Problem Statement

Let us consider a linear time-invariant process $G(s)$ with an available manipulable input u and a measurable output y, which can be affected by any disturbance. We assume that we can model the effect of disturbances as an additive signal added to the manipulable input, acting as an actuator disturbance signal d. The measurement is assumed to be affected by a noise signal v, which we consider high frequency and Gaussian. Therefore, the process is modelled as

$$y(s) = G(s)\,(u(s) + d(s)) + v(s). \tag{1}$$

We express the transfer function $G(s)$ as

$$G(s) = \frac{K s^{n_d} e^{-Ts} \prod_{i=1}^{n_\beta}(1+\beta_i s) \prod_{i=1}^{n_\delta}(1-\delta_i s)}{s^{n_i} \prod_{i=1}^{n_\tau}(1+\tau_i s)}, \tag{2}$$

where $n_i = 1$ if the system has an integrator and $n_i = 0$ if not, and $n_d = 1$ if the system has a derivative, and $n_d = 0$ if not. K is the process gain, β_i are the time constants of the half-left zeros in the complex plane ($\Re(\beta_i) > 0$) and δ_i the ones for those in the half-right plane ($\Re(\delta_i) > 0$). T is the dead time and τ_i the time constants of both the stable and unstable poles. The complex poles are also assumed to be represented in this general notation and, in that case, we would have a couple of conjugate τ_i complex values. We assume that the transfer function $G(s)$ is proper (i.e., $n_\beta + n_\delta + n_d \leq n_i + n_\tau$)

Remark 1. *Note that d in model (1) can be used to also model the effects of uncertainty on plant model $G(s)$. If the system can be modelled through*

$$y(s) = (G(s) + \Delta G(s))\,(u(s) + w(s)) + v(s), \tag{3}$$

where $\Delta G(s)$ refers to the non-modelled part of the plant, and w to the unknown disturbances, one only needs to identify d as the variable that covers the signal

$$d(s) = w(s) + G(s)^{-1}\Delta G(s)\,(u(s) + w(s)),$$

see [13].

Remark 2. *Note that d in model (1) can be used to also model the effects of a disturbance that enters in a different channel somewhere between the input and output. For instance, if the system can be modelled through*

$$y(s) = G_y(s)\,(G_u(s)\,u(s) + G_w(s)\,w(s)) + v(s), \tag{4}$$

where w refers to the unknown disturbances, one only needs to identify d as the variable that covers the signal

$$d(s) = \frac{G_w(s)}{G_u(s)}\,w(s),$$

and $G(s)$ the system composed by $G(s) = G_y(s)\,G_u(s)$.

We assume that the disturbance is persistent and cyclic with a given periodicity. We assume this disturbance as an uncertain signal, but we model its behaviour for analysis and design purposes as a slow time-varying term plus n_ω oscillatory terms

$$d(t) = d_0(t) + \sum_{i=1}^{n_\omega} d_i\,\sin(\omega_i\,t + \theta_i)$$

The term $d_0(t)$ can be assumed to be the addition of a constant term and a ramp with low slope ($d_0(t) = c_0 + c_1 t$). We assume that the frequencies are ordered in increasing order ($\omega_i < \omega_{i+1}$). If the signal has only one dominant frequency, the terms ω_i must be interpreted as the harmonic frequencies of the Fourier Series of the signal (i.e., $\omega_i = i \cdot \omega_1$, and ω_1 would be the main frequency).

The main objectives of this paper are

- To build a model-based estimator of the disturbance $d(t)$ using continuous transfer functions and few tuning parameters.
- To develop an implementation strategy that allows to easily add new oscillatory terms to the observer, to estimate different frequency components.
- To provide explicit relationships between tuning parameters and performance indices.

3. Disturbance Estimator Structure

In this Section we present our proposal for the Disturbance Observer (DO) and we justify the reasons that led us to adopt its structure, based in the fulfilment of the performance requirements defined below. We propose the general DO of the figure 1, composed of the transfer functions $H_u(s)$ and $H_y(s)$, so that the disturbance estimation is

$$\hat{d}(s) = H_u(s)u(s) + H_y(s)y(s), \tag{5}$$

where $H_u(s)$ and $H_y(s)$ are to be defined. Considering (1), we can express this estimation as

$$\begin{aligned}\hat{d}(s) \;=\; & H_y(s)G(s)d(s) + (H_u(s) + H_y(s)G(s))\,u(s) + \\ & + H_y(s)v(s),\end{aligned} \tag{6}$$

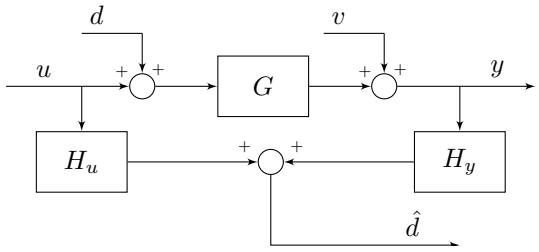

Figure 1: System with disturbance Estimator

where we observe the influence of input, disturbance, and noise on the estimation.

We define the disturbance estimation error as $\tilde{d}(s) = d(s) - \hat{d}(s)$ so

$$\begin{aligned}\tilde{d}(s) &= [1 - H_y(s)G(s)]\, d(s) - \\ &\quad - [H_u(s) + H_y(s)G(s)]\, u(s) - \\ &\quad - H_y(s)v(s). \end{aligned} \tag{7}$$

For optimal disturbance estimation, the objective is to minimize the disturbance estimation error $\tilde{d}$ for a given metric. In presence of disturbance d, this means that we want ideally $\hat{d} = d$. In presence of noise v and no disturbance, this means ideally $\hat{d} = 0$. This approach is slightly different to the residual approach commonly used in fault detection, where the objective is to maximize residual sensitivity to disturbance d and minimize residual sensitivity to noise v.

3.1. Initial analysis

The choice of a structure for $H_u(s)$ and $H_y(s)$ is based on the fulfilment of some desirable requirements for the DO. We define the following indicators to evaluate the performance of the DO with respect to the three exogenous signals of the system: the disturbance d, the input u and the noise signal v.

The proposed indicators are the following[1]:

A1. The steady-state disturbance estimation error versus step disturbance, defined as

$$\lim_{t\to\infty} \tilde{d}(t) = \lim_{s\to 0} (1 - H_y(s)G(s)) \tag{8}$$

A2. The steady-state disturbance estimation error under sinusoidal disturbances, defined as the frequency response of $[1 - H_y(s)G(s)]$ evaluated at each of the frequencies that define the periodic signal, i.e., the set

$$1 - H_y(j\,\omega_i)G(j\,\omega_i), \quad i = \{1, \ldots, N\}.$$

If $H_y(s)$ fulfils $1 - H_y(j\,\omega_i)G(j\,\omega_i) = 0$, the steady state error under sinusoidal disturbances of frequency ω_i is null.

[1]We use the final value theorem: $\lim_{t\to\infty} x(t) = \lim_{s\to 0} sX(s)$

A3. The noise effect, which according to (7) and assuming the noise as a high frequency signal is approximated by

$$\lim_{s\to\infty} -H_y(s).$$

A4. The sensitivity from the system input $u(s)$, defined with the $\mathcal{H}_\infty$ norm

$$\|H_u(s) + H_y(s)G(s)\|_\infty .$$

We look for a simple structure for $H_u(s)$ and $H_y(s)$ that achieves a satisfactory performance in terms of the previous indicators. Specifically, the next requirements must be fulfilled:

B1. $H_u(s)$ and $H_y(s)$ must be stable, proper, and causal (realizable). This also ensures a finite noise amplification, according to **A**3.

B2. Considering (7), $[1 - H_y(s)G(s)]$ and $[H_u(s) + H_y(s)G(s)]$ must be stable. This ensures a stable response of the disturbance observer from disturbances and manipulable inputs.

B3. $H_y(s)$ must fulfil $H_y(0)G(0) = 1$ and $H_y(j\,\omega_i)G(j\,\omega_i) = 1$ $(i = \{1, \ldots, N\})$ to ensure null steady-state disturbance estimation error under step and sinusoidal like signals, according to **A**1 and **A**2.

B4. The sensitivity from the system input must be bounded, i.e., $\|H_u(s) + H_y(s)G(s)\|_\infty \leq \epsilon,\ \epsilon \in \mathbb{R}^+$, according to **A**4.

In the next section, the selection of the structure of $H_u(s)$ and $H_y(s)$ is justified, considering the previous requirements.

3.2. Structure choice

Considering the dynamics of the disturbance error expressed in (7), we could achieve

- perfect disturbance estimation if $1 - H_y(s)G(s) = 0$;
- perfect input decoupling if $H_u(s) + H_y(s)G(s) = 0$;
- perfect high frequency noise attenuation if $H_y(\infty) = 0$.

Obtaining perfect disturbance estimation through setting

$$H_y(s) = G(s)^{-1}$$

is incompatible with several of the requirements indicated before. As $G(s)$ is usually strictly proper, $H_y(s)$ would be non-proper; if $G(s)$ has right half plane zeros, $H_y(s)$ would be unstable; if $G(s)$ has some delay, then $H_y(s)$ would be non-causal.

On the other hand, obtaining perfect noise attenuation would imply $H_y(s)$ being strictly proper, which is incompatible with perfect disturbance estimation, as $G(s)^{-1}$ will

never be strictly proper. We see here that in the design of the transfer function $H_y(s)$ there is a trade-off between achieving perfect disturbance estimation and noise attenuation.

However, once $H_y(s)$ is designed, achieving perfect input decoupling is possible by setting $H_u(s)$ to be

$$H_u(s) = -H_y(s)G(s). \tag{9}$$

With the same goal of input decoupling, one can explore the design of $H_u(s)$ and then set $H_y(s)$ to fulfil

$$H_y(s) = -H_u(s)G(s)^{-1}.$$

In any case, $H_u(s)$ and $H_y(s)$ fulfilling (9) and requirement B3, implies that $H_u(s)$ must satisfy

$$\begin{cases} H_u(0) = -1, \\ H_u(j\omega_i) = -1, \qquad i = 1, \ldots, n_\omega. \end{cases}$$

Note that once $H_y(s)$ and $H_u(s)$ are set to fulfil $H_u(s)+H_y(s)G(s) = 0$ and the estimator is implemented, the dynamics of the disturbance estimation and estimation error are reduced to

$$\hat{d}(s) = H_y(s)G(s)d(s) + H_y(s)v(s), \tag{10}$$

and

$$\tilde{d}(s) = [1 - H_y(s)G(s)]\, d(s) - H_y(s)v(s). \tag{11}$$

Writing these expressions in terms of $H_u(s)$, one obtains

$$\begin{aligned} \hat{d}(s) &= -H_u(s)d(s) - H_u(s)G(s)^{-1}v(s), \\ \tilde{d}(s) &= [1 + H_u(s)]\, d(s) + H_u(s)G(s)^{-1}v(s). \end{aligned} \tag{12}$$

Considering the fulfilment of (9), we discuss in the following section the structure for each transfer function $H_u(s)$ and $H_y(s)$ to achieve an implementation that allows the estimation of each frequency component of the disturbance signal and that uses comprehensive tuning parameters.

3.3. Decomposition for implementation

To achieve a simpler implementation based on the use of series and cascade operations with transfer functions that include recognizable terms, we propose to implement $H_u(s)$ as

$$H_u(s) = -1 + \prod_{i=0}^{n_\omega} (1 + H_{u,i}(s)), \tag{13}$$

where each $H_{u,i}(s)$ $(i = 0, \ldots, n_\omega)$ will be defined to fulfil $H_{u,i}(j\omega_i) = -1$ (i.e., to ensure null steady state error for each of the frequency components of d), to be stable, proper, and causal (with the aim of being implementable). Note that if each $H_{u,i}(s)$ leads to -1 at $s = j\omega_i$, for every ω_i of interest, then, $H_u(s)$ will lead to -1, as desired, when $s = j\omega_i$ for each ω_i of interest. On the other hand, we decide to implement $H_y(s)$ as

$$H_y(s) = \sum_{i=0}^{n_\omega} \left(H_{y,i}(s) \cdot \prod_{j=i+1}^{n_\omega} (1 + H_{u,j}(s)) \right) \tag{14}$$

where each $H_{y,i}(s)$ will be defined to be stable, proper, and causal. When $i = n_\omega$, the term in the product must be interpreted as 1. Figure 2 shows the block diagram that implements the proposed disturbance observer with simple transfer function blocks. It is straightforward to demonstrate that the proposed term decomposition satisfies $H_u(s) + G(s)H_y(s) = 0$, i.e., null process input sensitivity.

To define with more detail each term $H_{u,i}(s)$ and $H_{y,i}(s)$ that conforms $H_u(s)$ and $H_y(s)$, let us now decompose $G(s)$ as

$$G(s) = G_I(s)G_N(s),$$

where

$$G_I(s) = \frac{K \prod_{i=1}^{n_\beta}(1 + \beta_i s)}{s^{n_i} \prod_{i=1}^{n_\tau}(1 + \tau_i s)},$$

$$G_N(s) = s^{n_d} e^{-Ts} \prod_{i=1}^{n_\delta}(1 - \delta_i s).$$

$G_I(s)$ contains the part of $G(s)$ whose inverse leads to an stable and causal system, and $G_N(s)$ the part whose inverse leads to an unstable or non-causal system.

We propose to use a set of transfer functions $H_{u,i}(s)$ $(i = 0, \ldots, n_\omega)$ defined as

$$H_{u,i}(s) = -F_i(s)G_N(s), \tag{15}$$

and a set of transfer functions $H_{y,i}$ $(i = 0, \ldots, n_\omega)$ defined as

$$H_{y,i}(s) = F_i(s)G_I^{-1}(s), \tag{16}$$

where $F_i(s)$ is the filter such that

$$-F_i(j\omega_i)G_N(j\omega_i) = -1.$$

Note that the proposed set of transfer functions satisfies

$$H_{u,i}(s) + G(s)H_{y,i}(s) = 0$$

for each $i = 0, \ldots, n_\omega$, i.e., $H_{y,i}(s)$ can be rewritten as

$$H_{y,i}(s) = -H_{u,i}(s)G(s)^{-1}.$$

With these definitions, $H_y(s)$ in (14) can be rewritten with the operations detailed in Appendix Appendix A as

$$\begin{aligned} H_y(s) &= -\sum_{i=0}^{n_\omega} G(s)^{-1} H_{u,i}(s) \prod_{j=i+1}^{n_\omega} (1 + H_{u,i}(s)) \\ &= G(s)^{-1} \left(1 - \prod_{i=0}^{n_\omega} (1 + H_{u,i}(s)) \right) \end{aligned} \tag{17}$$

as each $H_{y,i}(s)$ fulfils $H_{y,i}(s) = -G(s)^{-1}H_{u,i}(s)$ by the proposed structure. With this, we have demonstrated that the proposed structure fulfils the perfect input decoupling condition $H_u(s) + G(s)H_y(s) = 0$. As seen in figure 2, our proposal allows to implement the observer as independent transfer functions, which makes it suitable to be easily implemented in industrial control systems. Note that each group marked in grey in the figure, corresponding to each term of the observer composed of the pair $H_{u,i}(s)$ and $H_{y,i}(s)$, can be included independently so that the user can plug as many terms as required, to estimate new frequency components, without any consideration on the already implemented terms.

Once we have discussed the internal structure of $H_u(s)$ and $H_y(s)$ that leads to fulfilment of (9), next we discuss the construction of filters $F_i(s)$ for implementability and estimation of each frequency term in $d(s)$.

3.4. Filter choice

In the following we define filters $F_i(s)$ (included in $H_{u,i}(s)$ and $H_{y,i}(s)$) to achieve disturbance estimation at the frequencies of interest, as well as ensuring that transfer functions $H_{u,i}(s)$ and $H_{y,i}(s)$ are realizable (stable, proper, and causal).

If the relative degree of $G_I(s)$ (given by $d_I = n_i + n_\tau - n_\beta$) is greater than zero, its inverse will not be proper. This will commonly happen with usual transfer functions (with more order in the denominator than half left plane zeros). On the other hand, the order of the numerator of $G_N(s)$, $n_\delta + n_d$ will be usually lower or equal than d_I. Therefore, the order of $F_i(s)$ must be at least

$$n_F = \max(d_I, n_\delta + n_d) \tag{18}$$

to guarantee that both $H_{y,i}(s)$ and $H_{u,i}(s)$ are realizable. The most common case in practice will be

$$n_F = d_I = n_i + n_\tau - n_\beta. \tag{19}$$

3.4.1. Low pass term

First, we define the filter for $i = 0$ ($\omega_0 = 0$, i.e., to observe the steady state or average value of signal d). To achieve a proper transfer function $H_{y,0}(s)$, we propose to include a pole with multiplicity n_F, i.e.,

$$F_0(s) = \frac{1}{(1+\alpha\, s)^{n_F}}. \tag{20}$$

With this, $H_{y,0}(s)$ is defined by

$$H_{y,0}(s) = \frac{G_I(s)^{-1}}{(1+\alpha s)^{n_F}} = \frac{s^{n_i}\prod_{i=1}^{n_\tau}(1+\tau_i s)}{K\,(1+\alpha s)^{n_F}\prod_{i=1}^{n_\beta}(1+\beta_i s)}, \tag{21}$$

and $H_{u,0}(s)$ by

$$H_{u,0}(s) = \frac{-G_N(s)}{(1+\alpha s)^{n_F}} = \frac{-s^{n_d}e^{-Ts}\prod_{i=1}^{n_\delta}(1-\delta_i s)}{(1+\alpha s)^{n_F}}. \tag{22}$$

Note that α is the unique tuning parameter in this term, to be defined.

3.4.2. Resonant terms

Next, we define the filters for $i = 1, \ldots, n_\omega$ (i.e., to observe the oscillatory components d). We propose initially

$$F_i(s) = \left[\frac{A_i + B_i s}{s^2 + 2\xi_i w_i s + w_i^2}\right]^{n_F},$$

with A_i, B_i, $0 < \xi_i < 1$ and w_i to be defined next. Then, in order to satisfy $F_i(j\omega_i)G_N(j\omega_i) = 1 + 0j$ and that the magnitude of the frequency response of $F_i(s)G_N(s)$ has a maximum at $s = j\omega_i$, i.e.,

$$\left.\frac{\partial|F_i(j\omega)G_N(j\omega)|}{\partial\omega}\right|_{\omega=\omega_i} = 0,$$

the values for w_i, A_i and B_i are chosen as

$$w_i = \omega_i, \quad A_i = \frac{2\xi_i\omega_i^2\,\sin\phi_i}{|G_N(j\omega_i)|^{\frac{1}{n_F}}}, \quad B_i = \frac{2\xi_i\omega_i\,\cos\phi_i}{|G_N(j\omega_i)|^{\frac{1}{n_F}}},$$

being ϕ_i the angle

$$\phi_i = \frac{1}{n_F}\arg(G_N(j\omega_i)). \tag{23}$$

Note that ξ_i is the tuning parameter corresponding to the i-th resonant term, to be defined. With these considerations, $H_{y,i}(s)$ is defined by

$$H_{y,i}(s) = \frac{G_I(s)^{-1}(A_i + B_i s)^{n_F}}{(s^2 + 2\xi_i w_i s + w_i^2)^{n_F}} = \\ = \frac{(A_i + B_i s)^{n_F} s^{n_i}\prod_{i=1}^{n_\tau}(1+\tau_i s)}{K\,(s^2 + 2\xi_i w_i s + w_i^2)^{n_F}\prod_{i=1}^{n_\beta}(1+\beta_i s)}, \tag{24}$$

and $H_{u,i}(s)$ by

$$H_{u,i}(s) = \frac{-G_N(s)(A_i + B_i s)^{n_F}}{(s^2 + 2\xi_i w_i s + w_i^2)^{n_F}} = \\ = \frac{-(A_i + B_i s)^{n_F} s^{n_d} e^{-Ts}\prod_{i=1}^{n_\delta}(1-\delta_i s)}{(s^2 + 2\xi_i w_i s + w_i^2)^{n_F}}. \tag{25}$$

The tuning of each resonant term only requires setting a single parameter, ξ_i.

3.4.3. First order plus time delay case

In the case of a first order plus time delay model (FOTD), a model commonly used in process industry, where

$$G(s) = \frac{Ke^{-Ts}}{1+\tau s},$$

the previous transfer functions become explicitly

$$H_{y,0}(s) = \frac{1}{K}\frac{(1+\tau s)}{(1+\alpha s)}, \qquad H_{u,0}(s) = \frac{-e^{-Ts}}{1+\alpha s},$$

$$H_{y,i>0}(s) = \frac{(1+\tau s)2\xi_i\omega_i(\sin(-\omega_i T)\omega_i + \cos(-\omega_i T)s)}{K(s^2 + 2\xi_i\omega_i s + \omega_i^2)},$$

$$H_{u,i>0}(s) = \frac{-e^{-Ts}2\xi_i\omega_i(\sin(-\omega_i T)\omega_i + \cos(-\omega_i T)s)}{(s^2 + 2\xi_i\omega_i s + \omega_i^2)}.$$

Note that in the FOTD case $n_F = 1$.

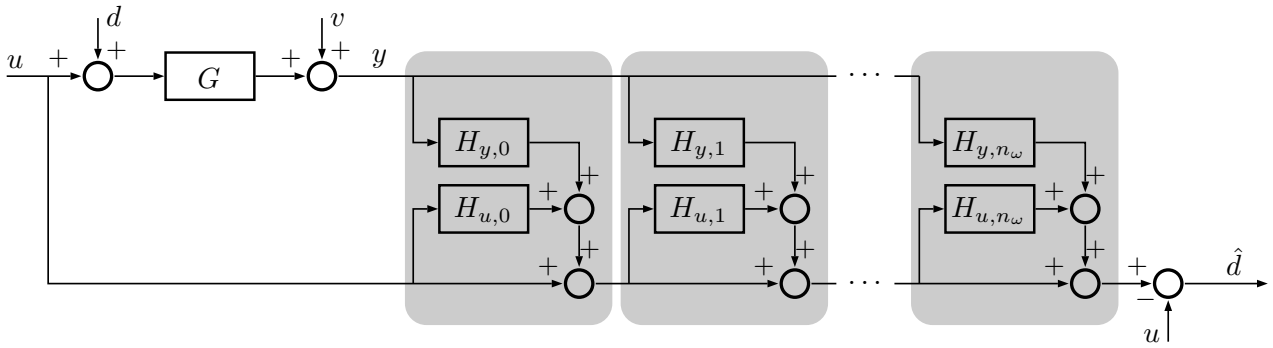

Figure 2: Block diagram of the proposed additive-cascade structure for the multi-resonant observer

3.5. Sequential interpretation

The proposed implementation can be interpreted as a sequence of simple disturbance observers where each of them is devoted to estimate a given frequency component of the disturbance, using those components already estimated. For interpretation issues, let us assume that the implementation is done in increasing terms of frequency (i.e., each filter $H_{u,i}(s)$ and $H_{y,i}(s)$ refers to an increasing frequency as i grows).

Let us decompose the disturbance to be estimated as a summation of signals

$$d(s) = d_0(s) + d_1(s) + d_2(s) + \cdots + d_{n_\omega}(s).$$

where d_0 refers to the low frequency component of the signal (i.e., constant or slow ramp-like variations), and d_i ($i = 1, \ldots, n_\omega$) refers to the oscillatory component with frequency ω_i. In its first stage, the proposed implementation can be interpreted as an estimator for d_0 from the known input u and measured output y, i.e.,

$$\hat{d}_0(s) = H_{u,0}(s)u(s) + H_{y,0}(s)y(s).$$

Once we have an estimate for d_0, in a second stage, we can interpret that we estimate d_1 from inputs u (known) and d_0 (estimated in the previous stage), and y, i.e.,

$$\hat{d}_1(s) = H_{u,1}(s)(u(s) + \hat{d}_0(s)) + H_{y,1}(s)y(s).$$

With this, any following stage can be interpreted as an estimation of d_i from inputs u (known) and $d_0, \ldots, d_{i-1}$ (estimated) and output y, i.e.,

$$\hat{d}_i(s) = H_{u,i}(s)\left(u(s) + \sum_{j=0}^{i-1} \hat{d}_j(s)\right) + H_{y,i}(s)y(s).$$

Finally, the estimate for disturbance d will be the summation of each of the estimated components, $\hat{d}(s) = \sum_{i=0}^{N} \hat{d}_i(s)$.

The idea is that the estimator for component d_0 will be designed to assure proper steady state estimation under step and ramp disturbances, and the rest of the filters will be devoted to estimate each of the frequencies that were not contemplated by the previous filter (each of the frequencies of the oscillatory disturbances).

4. Disturbance estimator tuning

In the previous section we have proposed a structure for the transfer functions $H_y(s)$ and $H_u(s)$. In this section, we analyse how to tune the different parameters α and ξ_i.

4.1. Disturbance estimator error analysis

First, let us rewrite the disturbance estimation error dynamics (7) including the proposed disturbance estimator structure, given by (21) and (22). Disturbance estimation error becomes

$$\begin{aligned}\tilde{d}(s) \quad &= \left[\prod_{i=0}^{n_\omega}(1 + H_{u,i}(s))\right] d(s) - \\ &- \left[\sum_{i=0}^{n_\omega}\left(H_{y,i}(s) \cdot \prod_{j=i+1}^{n_\omega}(1 + H_{u,j}(s))\right)\right] v(s),\end{aligned} \tag{26}$$

where we appreciate the cancellation of the effect of input u over the disturbance estimation error, and that the poles defining dynamics of the disturbance estimation error are the ones included in the filter terms ($s = -1/\alpha$ for the low pass term and $s = -\xi_i\omega_i \pm j\sqrt{\xi_i^2 - 1}\,\omega_i$ for the resonant terms, both with multiplicity n_F).

To present expressions that help to the filter design, now we assume the following assumptions. First, we assume that each component of the product defining the estimation error due to disturbances (see (26)) implies both a transitory and steady-state behaviour for any signal. We also assume that the frequency response of each component will be negligible for other frequencies, i.e., for $i = 0, \ldots, n_\omega$,

$$\begin{cases} F_i(j\omega)G_N(j\omega) = 1 + 0j, & \omega = \omega_i \\ 0 \leq |F_i(j\omega)G_N(j\omega)| \ll 1, & |\omega - \omega_i| > \epsilon \end{cases} \tag{27}$$

for some ϵ, and where ω_0 must be understood as frequency zero (referring to the term estimating the constant term of the disturbance).

4.1.1. Convergence of the estimation error

Given the previous fact, we use the dynamics of the transient part of the estimation error signal to assess the behaviour of each component of the estimator. The disturbance estimation error due to disturbances can be expressed as

$$\tilde{d}(s) = \left[\prod_{i=0}^{n_\omega}(1 - F_i(s)G_N(s))\right] d(s). \tag{28}$$

On one hand, we can obtain some metrics of the performance from the assessment of system and signal norms in the previous expression (see Appendix B the detail on some discarded performance indices). Due to the oscillatory nature of the signals, and due to the complex expressions that may be derived for high order, we avoid the assessment with this method.

On the other hand, we can assess the time response via the poles effect. The time expression of the error signal $\tilde{d}(t)$ will be composed of a summation of terms related to each of the denominators of the elements $(1-F_i(s)G_N(s))$. Since $G_N(s)$ has no poles, the denominator coincides with the one in $F_i(s)$. The elements in $G_N(s)$ (time delay and non-minimum phase terms) will imply a delay in the estimation in the order of

$$t_d = \sum \delta_i + T. \tag{29}$$

We see then that we can consider the transient time due to $F_i(s)$ as the metric to asses the behaviour of each of the filters, since the effect of the non invertible part is common to each of the terms. In that sense, we will assume that the settling time of each component i is in the order of magnitude

$$t_{s,i} \lessapprox \frac{1.4 + 2.53\, n_F^{0.8}}{\sigma_i}, \tag{30}$$

where σ_i refers to the absolute value of the real part of the poles (see Appendix C). This approximated equation has been obtained from the step response of several multiple poles transfer functions, computing the settling time and fitting a function of n_F. In the case of the low-pass filter, this is $\sigma_0 = \frac{1}{\alpha}$, and in the resonant terms, this is $\sigma_{i>0} = \xi_i\omega_i$ (for $\xi < 1$).

4.1.2. Attenuation of the measurement noise

On the other hand, the absolute value of the high frequency response of the transfer function $\frac{\hat{d}(s)}{v(s)} \equiv H_y(s)$ is determined by the limit

$$\lim_{s\to\infty} H_y(s) = \lim_{s\to\infty}\left[\sum_{i=0}^{n_\omega}\left(H_{y,i}(s)\cdot\prod_{j=i+1}^{n_\omega}(1+H_{u,j}(s))\right)\right] = \\ = \sum_{i=0}^{n_\omega}\left(H_{y,i}(\infty)\right), \tag{31}$$

where $\lim_{s\to\infty} H_{u,j}(s) = 0$ has been considered. The previous limit exists as $H_y(s)$ is strictly proper, i.e., it has direct gain, due to the value selected in n_F (see (18) and (19)).

Assuming that the noises are high frequency signals, we use the previous limit as the indicator for noise amplification, and the variance of the estimation due to measurement noises is

$$\sigma_d^2 = \left(\lim_{s\to\infty} H_y(s)\right)^2 \sigma_v^2 \tag{32}$$

where $\sigma_d^2 = var(\hat{d})$ and $\sigma_v^2 = var(v)$.

4.1.3. Summary of error analysis

Here we summarize several indicators for both steady state and transient error that are useful for design purposes.

- Steady state error under a step in d:

$$\lim_{t\to\infty}\tilde{d}(t) = 0.$$

- Steady state error under a ramp in d:

$$\lim_{t\to\infty}\tilde{d}(t) = \\ = \left(n_F\,\alpha + \sum\delta_i + T\right)\prod_{i=1}^{n_\omega}\left(1 - \frac{(2\xi_i\,\sin(\phi_i))^{n_F}}{|G_N(j\omega_i)|}\right). \tag{33}$$

- Steady state error for sinusoidal d of frequency ω_i:

$$\lim_{t\to\infty}\tilde{d}(t) = 0.$$

- Settling time of the term related to frequency $\omega_0 = 0$ (applying equation (30)):

$$t_{s,0} \lessapprox (1.4 + 2.53\, n_F^{0.8})\alpha + \sum\delta_i + T. \tag{34}$$

- Settling time of the term related to frequency ω_i:

$$t_{s,i} \lessapprox \frac{1.4 + 2.53\, n_F^{0.8}}{\xi_i\omega_i} + \sum\delta_i + T. \tag{35}$$

- High frequency measurement noise amplification (related to high frequency noise v):

$$\lim_{s\to\infty} H_y(s) = \\ = \frac{\prod\tau_i}{K\prod\beta_i}\left(\frac{1}{\alpha^{n_F}} + \sum_{i=1}^{n_\omega}\frac{(2\xi_i\omega_i\,\cos(\phi_i))^{n_F}}{|G_N(j\omega_i)|}\right). \tag{36}$$

The value of the tuning parameters α and ξ_i have an impact on the measurement noise amplification as well as on the transient tracking error of the disturbance estimation.

4.2. Tuning rules

From the previous metrics we realize that a high value of α reduces the noise effect but, under step disturbances, slows the disturbance signal tracking, while a lower α speeds up the disturbance signal tracking but increases the noise effect. In the same sense, we get less harmful effect from

noise if we use lower values of ξ_i but that slows down disturbance tracking under sinusoidal disturbances. In the same sense, under ramp-like disturbances, we have lower error when using lower α and higher ξ_i values. Therefore, there is a trade-off between tracking speed and noise effect and the tuning aims at achieving a compromise between those two factors. Therefore, the tuning can be based in deciding the noise amplification effect or the tracking speed (tracking error in the case of expected ramp-like disturbances).

The right number of resonant terms to include in the multi-resonant observer is related with the disturbance nature, i.e., the periodic signal in terms of the number of significant harmonics. Since we suppose d is unknown, this may be difficult to know, so we recommend trying different options in a training dataset.

The tuning procedure can be based in deciding a total noise amplification N or a settling time t_s. According to (36), a certain noise amplification can be achieved with several combinations of α and ξ_i. The settling time, according to (34) and (35), can be set differently for each frequency component of the disturbance. Since the amplitude of each frequency component present in the disturbance signal is unknown, we propose in the following several alternatives. The proposed tuning procedure is as follows:

1. Gather a data set $\mathcal{X} = (u(t), y(t))$ $(t \in [0, T])$ around a given operating point with sufficient excitation in input $u(t)$ for identification purposes.
2. Identify the process to obtain a model $G(s)$ of the form (2).
3. From a model $G(s)$, factorize it into $G_I(s)$ and $G_N(s)$, so that $G_I(s)$ contains the part of $G(s)$ whose inverse leads to an stable and causal system, and $G_N(s)$ the part whose inverse leads to an unstable or non-causal system.
4. Compute $n_F = \max(d_I, n_\delta + n_d)$, according to (18).
5. Obtain the main frequency ω_1 of the disturbance signal. For instance, if it is related to some natural daily phenomena, $\omega_1 = \frac{2\pi}{24 \cdot 3600}$ rad/s.
6. Select a number n_ω of resonant terms, ideally small for simplicity, and compute the frequencies ω_i. Normally, if there is no information on the frequency spectrum of the disturbance signal, the harmonic frequencies are chosen w.r.t. ω_1, i.e., $\omega_i = i \cdot \omega_1$, $i > 1$.
7. Compute $\phi_i = n_F^{-1} \arg(G_N(j\omega_i))$ for $i = 1, \ldots, n_\omega$, according to (23).
8. Decide a target for either total noise amplification N or a settling time t_s.
9. Select one of the following three alternatives:

(Alt. a) Set a noise weighting N_i for each term such that $\sum_{i=0}^{n_\omega} N_i = N$ and set

$$\alpha = \left(\frac{1}{N_i} \frac{\prod \tau_j}{K \prod \beta_j} \right)^{\frac{1}{n_F}}, \tag{37}$$
$$\xi_i = \left(N_i \frac{K \prod \beta_j}{\prod \tau_j} \frac{|G_N(\omega_i j)|}{(2\omega_i \cos(\phi_i)^{n_F})} \right)^{\frac{1}{n_F}}, \; i > 0$$

If no information on how to weight each term is available, one can set, for instance, an *equitable noise weighting* by choosing $N_i = \frac{N}{n_\omega + 1}$ for all the terms $(i = 0, \ldots, n_\omega)$.

(Alt. b) Set a settling time $t_{s,i}$ for each term such that $t_{s,i} \leq t_s$ and set

$$\alpha = \frac{1}{(1.4 + 2.53\, n_F^{0.8})} \left[t_{s,i} - \sum \delta_j - T \right], \tag{38}$$
$$\xi_i = \frac{(1.4 + 2.53\, n_F^{0.8})}{\omega_i} \left[t_{s,i} - \sum \delta_j - T \right]^{-1}, \; i > 0$$

Again, if no information on how to tune each term is available, one can apply an *equitable settling time weighting* by choosing $t_{s,i} = t_s$ for all the terms $(i = 0, \ldots, n_\omega)$.

(Alt. c) If some input-output data set is available to perform a simulation of the observer, one can apply an *optimal weighting*. Here, α and ξ_i are obtained by performing an optimization over the dataset trying to minimize some norm of the estimated output error with the constraint of either total noise amplification lower than a given N or either a settling time lower than a given t_s for each of the filter terms. First, one must construct the observer with the proposed structure and apply it over the data set to obtain the estimated disturbance. Let us call the data set $\mathcal{Y} = (u(t), y(t))$ $(t \in [0, T])$, let us assume that it covers several oscillations of the main frequency ω_1 (at least three complete oscillations, i.e., $T > 3 \cdot \frac{2\pi}{\omega_1}$), and let us write the disturbance estimate as

$$\hat{d}(s) = H_u(s)u(s) + H_y(s)y(s)$$

leading to a data set of estimated disturbance values $\hat{d}(t)$. Then, one must reconstruct the output with

$$\hat{y}(s) = G(s)(u(s) + \hat{d}(s)),$$

leading to a data set of estimated output values $\hat{y}(t)$. Note that this reconstructed output can be rewritten as

$$\hat{y}(s) = [G(s)(1 + H_u(s))]u(s) + [G(s)H_y(s)]y(s),$$

and, therefore, it can be obtained just adding the simulated output of the linear systems $G(s)(1+H_u(s))$ and $G(s)H_y(s)$ using the acquired datasets $u(t)$ and

$y(t)$, respectively, as inputs. With this, one can perform a search of the parameters α and ξ_i by minimizing, for instance

$$\int_0^T (y(t) - \hat{y}(t))^2 \, dt,$$

to minimize the integral of the squared error, where $y(t) - \hat{y}(t)$ represents the difference between the output measurements and the reconstructed output (that considers both known input u and estimated unknown input $\hat{d}$). Another index can be, for instance $\int_0^T |y(t) - \hat{y}(t)| \, dt$ to minimize the integral of the absolute error.

Note that data set $\mathcal{Y}$ must be acquired only once to validate the design, and it is independent of the number of resonant terms n_ω being explored.

10. Return to step 6 and include one extra resonant term. Repeat all the steps and compare with previous results. Do this until acceptable performance is achieved.

To achieve a faster response time of those terms whose weight in terms of amplitude is larger in the disturbance signal, we should use low values of α (if the slow dynamics is dominant), or high values in the ξ_i whose frequencies are dominant. To achieve this, we allow more noise amplification in those terms. In this sense, optimal weighting depends on the amplitude of each component in the disturbance signal. Since this may be unknown, this optimization can be performed through simulations over the application data, by setting aside a training dataset. In all the cases, we must satisfy $\alpha > 0$ and $\xi_i > 0$. With respect the selection of the number of resonant terms, one must notice from equation (36) the existing trade off between the achievable noise attenuation and the inclusion of resonant terms. Each new resonant term will lead to more noise amplification. Or, in other words, if we want to include a new resonant term while keeping a given noise attenuation, we will have a slower estimator response, as it will require well increasing α or decreasing some of the ξ_i values.

4.3. Addressing nonlinear systems

One of the limitations of the proposed approach is that it assumes a fixed operating point where a linear model can be obtained. This is the case for most real applications, where the operating point usually do not change over time. However, when the operating point changes over time it changes usually amongst a short finite set of different (and close) operating points. Furthermore, if that change is slower than the achievable dynamics in the estimator, one approach to overcome this limitation is to design a different disturbance observer at each operating point and run in parallel a bank of observers. Then, the valid disturbance estimate will be the one obtained with the model of the actual operating point. This approach would lead to results similar to those ones developed by means of nonlinear models, specially those ones that mainly model the changing static gain of the process along the operating points. In order to apply this bank of estimators technique, one should modify the tuning rules repeating all the steps for each operating point.

5. Control applications of the disturbance observer

5.1. Application in pure feed forward control

One of the main applications of the disturbance estimation is its use to manipulate the actuator to reject the disturbance effect on an output signal of interest. For instance, one can obtain the control action as the summation of a given open loop control action u_c (to have some average value in the output, for instance), minus the estimate $\hat{d}$ leading to

$$u(t) = u_c(t) - \hat{d}(t). \tag{39}$$

The measured output is then given by

$$y(s) = G(s)\, u_c(s) + G(s)\,(1 + H_u(s))\, d(s) + (1 + H_u(s))v(s)$$

where the fact $H_u(s) + G(s)\, H_y(s) = 0$ has been applied. Noting that $(1 + H_u(s))\, d(s)$ represents the disturbance estimation error, we see that its effect over the output is

$$\tilde{y}(s) = G(s)\,(1 + H_u(s))\, d(s) = G(s)\, \tilde{d}(s).$$

Therefore, the lower the disturbance estimation error, the lower its effect over the output, or the better the disturbance rejection in the output. Concisely, as the proposed disturbance observer has been demonstrated to estimate slow disturbances as well as the periodical components included in the observer terms, we can conclude that the feedforward of the disturbance estimation can significantly mitigate those disturbance terms on the output. In the case of ramp-like disturbances, the estimation error given by (33) in section 4.1.3, leads to a tracking error equal to (assuming unitary ramp)

$$\lim_{t\to\infty} \tilde{y}(t) = \tag{40}$$
$$K\left(n_F\,\alpha + \sum \delta_i + T\right) \prod_{i=1}^{n_\omega} \left(1 - \frac{(2\xi_i\, \sin(\phi_i))^{n_F}}{|G_N(j\omega_i)|}\right).$$

5.2. Application in disturbance observer control

The other main useful application of disturbance observers is its use within a closed-loop control through a feed-forward term, what is called Disturbance Observer Control (DOB). In that case, the control algorithm becomes

$$\hat{d}(s) = H_u(s)u(s) + H_y(s)y(s), \tag{41a}$$
$$u_c(s) = C(s)\,(r(s) - y(s))\,, \tag{41b}$$
$$u(s) = u_c(s) - \hat{d}(s). \tag{41c}$$

where $C(s)$ represents the controller transfer function (for instance, a PID controller), u_c represents the control action computed by the controller, and u is the total applied control action, that includes the feedforward term $-\hat{d}(s)$ to mitigate the disturbance effect on the system output. In this case, the measured output can be expressed as

$$y(s) = \frac{G(s)\,C(s)}{1+G(s)\,C(s)} r(s) + \frac{G(s)\,(1+H_u(s))}{1+G(s)\,C(s)} d(s) + \\ + \frac{1+H_u(s)}{1+G(s)\,C(s)} v(s) \quad (42)$$

or, equivalently (with $D(s) = 1 + G(s)\,C(s)$)

$$y(s) = \frac{G(s)\,C(s)}{D(s)} r(s) + \frac{G(s)}{D(s)} \tilde{d}(s) + \frac{1+H_u(s)}{D(s)} v(s) \quad (43)$$

From this transfer function it can be demonstrated (see [44, 45]) that this control structure is able to track without steady state error constant setpoints, constant and ramp-like disturbances, as well as sinusoidal disturbances (if the components are included in the disturbance observer). This is the main advantage of using this control structure. On the other hand, the sensitivity $S(s)$ function is

$$S(s) = S_0(s)(1 + H_u(s)), \quad (44)$$

$$S_0(s) = \frac{1}{1 + C(s)G(s)}, \quad (45)$$

where $S_0(s)$ denotes the conventional sensitivity function (when there is no estimated disturbance feedforward term). The robustness and oscillatory behaviour of the closed loop system can be assessed by means of the $\mathcal{H}_\infty$ norm of $S(s)$, i.e., the peak of the frequency response, $\|S(s)\|_\infty = \max_\omega |G(j\omega)|$. From this fact one can obtain the bound

$$\|S(s)\|_\infty \leq \|S_0(s)\|_\infty \cdot \|1 + H_u(s)\|_\infty \quad (46)$$

where $\|S_0(s)\|_\infty$ represents the sensitivity peak of the initial controller $C(s)$, and where the term $\|1 + H_u(s)\|_\infty$ represents the robustness worsening that can generate the use of the feedforwad term. The work [44] shows the trade-off between noise attenuation, disturbance mitigation and closed loop robustness in the case of disturbance observers that only include low pass filter terms. One of the conclusions is that, for a set of observers that have the same measurement noise attenuation, the higher the disturbance mitigation, the higher the sensitivity peak $\|S(s)\|_\infty$, i.e., better disturbance mitigation properties are at the cost of losing robustness. In fact, for the FOTD case, [44] shows the peak increase as a function of the ratio between the time constant α of the filter in $H_u(s)$ and the delay in the non-invertible part (T), i.e., $\frac{\alpha}{T}$, shown in table 1. Considering (13) we have that

$$\|1 + H_u(s)\|_\infty \leq \prod_{i=0}^{n_\omega} \|1 + H_{u,i}(s)\|_\infty, \quad (47)$$

i.e., we can consider that each term can worsen the robustness if $\|1 + H_{u,i}(s)\|_\infty > 1$. In the numerical example we will show the value $\|1 + H_u(s)\|_\infty$ to asses the disturbance estimation use as a feed forward in a closed loop system.

$\frac{\alpha}{T}$	$\|1 + H_u(s)\|_\infty$
0.1	1.95
1	1.4
10	1.1
100	1.01

Table 1: Increase in the sensitivity peak in DOB.

6. Comparison with other methods

Other approaches based on state space methods are based on obtaining first an augmented state space model that includes the system dynamics and the proposed disturbance dynamics (integrator to assume constant terms, and resonant one for oscillatory behaviour, see [46, 47]). From the initial system model

$$\dot{x} = A\,x + B\,(u + d); \qquad y = C\,x \quad (48)$$

and the disturbance model $d(t) = d_0(t) + \sum_{i=1}^{n_\omega} d_i(t)$ generated by

$$\dot{z} = A_z\,z; \qquad d = C_z\,z \quad (49)$$

where $z = [z_0^T\ z_1^T\ \cdots\ z_{n_\omega}^T]^T$, and

$$A_d = \begin{bmatrix} A_0 & & & 0 \\ & A_1 & & \\ & & . & \\ 0 & & & A_{n_\omega} \end{bmatrix},\ C_d = \begin{bmatrix} C_0 & C_1 & \cdots & C_{n_\omega} \end{bmatrix}$$

being $A_0 = 0,\ A_{i>0} = \begin{bmatrix} 0 & 1 \\ -\omega_i^2 & 0 \end{bmatrix},\ C_0 = 1,\ C_{i>0} = \begin{bmatrix} 1 & 0 \end{bmatrix}$

An extended model including internal dynamics and disturbance generation is expressed as

$$\xi = \bar{A}\,\xi + \bar{B}\,u; \quad y = \bar{C}\,\xi; \quad d = \bar{C}_z\,\xi$$

being $\xi = [x^T\ z^T]^T$ and

$$\bar{A} = \begin{bmatrix} A & B\,C_z \\ 0 & A_z \end{bmatrix},\ \bar{B} = \begin{bmatrix} B \\ 0 \end{bmatrix},\ \bar{C} = \begin{bmatrix} C & 0 \end{bmatrix},\ \bar{C}_z = \begin{bmatrix} 0 & C_z \end{bmatrix}$$

and where $\bar{C}_z$ allows to extract the disturbance value. With this, a disturbance observer can be defined as

$$\dot{\hat{\xi}} = \bar{A}\,\hat{\xi} + \bar{B}\,u + L(y - \bar{C}\,\hat{\xi}) \quad (50)$$

$$\hat{d} = \bar{C}_z\,\hat{\xi} \quad (51)$$

To apply this method in systems with delays, model(48) must include an approximation by means of Pade. In this case, if delays are approximate, the constraint $H_u(s) + G(s)H_y(s) = 0$ cannot be assured. On the other hand, the implementation through the resulting transfer functions will not allow access to the tuning parameters or online fine readjustment.

In the state space approach, several techniques are available to design the disturbance observer: pole placement, linear quadratic estimator, or optimization-based

approaches. In the case of linear quadratic estimator, one must fix matrices W and V representing the covariance of the state and measurement noises, respectively. These can be used as tuning parameters. If no information is known about W, one can set it as $W = \gamma \bar{C}_z^T \bar{C}_z$ (see [46]), being γ the unique tuning factor. Then, matrix $P = P^T > 0$ solving the algebraic Riccati equation

$$P\,\bar{A}^T + \bar{A}\,P - P\,\bar{C}^T\,V^{-1}\,\bar{C} + W = 0$$

must be obtained, leading to gain matrix $L = P\,\bar{C}^T\,V^{-1}$. On the optimization based approach [47], linear matrix inequalities must be developed to obtain a tractable numerical approach, leading to a more complex problem.

In the case of Pade approximation of the delays, one can evaluate the control action decoupling by evaluating the H_∞ norm of $H_u(s) + G(s)H_y(s)$.

7. Numerical example

To clarify and illustrate previous results, in this section we present a numerical example where we can observe the estimation performance of the proposed observer.

Let us consider a FOTD process that can be modelled as

$$G(s) = \frac{1}{(1+s)}e^{-0.5s}, \tag{52}$$

i.e., with $K = 1$, $\tau = 1$ and $T = 0.5$, and with time units expressed in seconds.

We want to test the performance of an observer configured by a low pass filter and one resonant term ($n_\omega = 1$), suitable to estimate periodic disturbances with a period of 5 seconds, i.e., $\omega_1 = 1.2566$ rad/s is the unique considered frequency. Considering the FOTD ($n_F = 1$) process model,

$$G_I(s) = \frac{1}{(1+s)},\ G_N(s) = e^{-0.5s},$$

$$|G_N(j\omega_1)| = 1,\ \phi_1 = arg(G_N(j\omega_1)) = -1.5270\,\text{rad}.$$

The transfer functions of the observer are defined by

$$\begin{aligned}
H_{y,0}(s) &= \frac{1}{K}\frac{(1+\tau s)}{(1+\alpha s)} = \frac{1+s}{(1+\alpha s)}, \\
H_{u,0}(s) &= \frac{-e^{-Ts}}{1+\alpha s} = \frac{-e^{-0.5s}}{(1+\alpha s)}, \\
H_{y,1}(s) &= \frac{(1+\tau s)2\xi_1\omega_1(\sin(-\omega_1 T)\omega_1 + \cos(-\omega_1 T)s)}{K(s^2 + 2\xi_1\omega_1 s + \omega_1^2)} \\
&= \frac{(1+s)\xi_1(-1.856 + 2.033s)}{s^2 + 2.5132\xi_1 s + 1.579}, \\
H_{u,1}(s) &= \frac{-e^{-Ts}2\xi_1\omega_1(\sin(-\omega_1 T)\omega_1 + \cos(-\omega_1 T)s)}{(s^2 + 2\xi_1\omega_1 s + \omega_1^2)} \\
&= \frac{(-e^{-0.5s})\xi_1(-1.856 + 2.033s)}{s^2 + 2.5132\xi_1 s + 1.579}.
\end{aligned} \tag{53}$$

To test the effect of the observer tuning in its performance, we have used two different values for α and ξ_1. First, in the low pass filter term, for a settling time of 20 seconds, using equation (34) one obtains $\alpha = 5$, and for $t_s = 80$ one obtains $\alpha = 20$. Second, in the resonant term, for $t_s = 13$, using equation (35) one obtains $\xi_1 = 0.25$, and for $t_s = 32$ one obtains $\xi_1 = 0.1$. We have numbered the different options as

$$\alpha_1 = 5, \quad \alpha_2 = 20, \quad \xi_{1,1} = 0.1, \quad \xi_{1,2} = 0.25.$$

The dynamics of disturbance estimation $\hat{d}$, under disturbance d, according to (12), defined by $-H_u(s)$, can be obtained by substituting the previous values for $H_{u,0}(s)$ and $H_{u,1}(s)$ in (13).

Figure 3 shows the Bode diagrams for the four combinations of α and ξ from the disturbance to the disturbance estimation. The behaviour of $-H_u(s)$ matches $-H_{u,0}(s)$ for the low frequencies and, as well as $-H_{u,1}(s)$, ensures a magnitude of 1 and a phase of 0^o in the desired frequency ω. We see how the value of α affects the low frequency response and the value of ξ_1 determines the peak width around ω_1. A wider peak implies better estimation for disturbance signals that are slightly different than the design frequency. Therefore, ξ_1 also influences the robustness against frequency value accuracy. Here we can see the degree of compliance of the assumption that the frequency response of each component is negligible for other frequencies (see (27)), i.e., the degree of interaction between frequency components of the observer.

Figure 4 presents the observer time response under a step disturbance in the four cases. The value of α affects the estimation speed, so that low values get faster responses compared with higher values. Due to the inclusion of a resonant estimator, we can see an overshooting response caused by $-H_{u,1}(s)$. The higher the value of ξ_1, the bigger the amplitude of the overshoot, but its dampening is faster.

Finally, figure 5 displays the observer time response under a sine disturbance with period $5s$, also in the four cases. The value of α has an impact on how the low pass term of the estimator, $-H_{u,0}(s)$, reacts to the periodic disturbance; more reaction is expected for low values of α. The value of ξ_1 affects the estimation speed. Faster estimation is achieved in the second case, with a higher value for ξ_1, but as we have seen in the previous sections, a drawback is that noise amplification is higher in that case.

Table 2 summarizes the obtained settling time versus step and ω_1 sine disturbances, the Integral Absolute Error (IAE) and the noise amplification. Best results for each indicator are highlighted in green. We can observe the trade-off between the indicators related to the tracking speed and those related with noise amplification. We also show the value $\|1 + H_u(s)\|_\infty$ as a measure of the robustness worsening index as indicated in (46). We can appreciate that the best results w.r.t. noise amplification

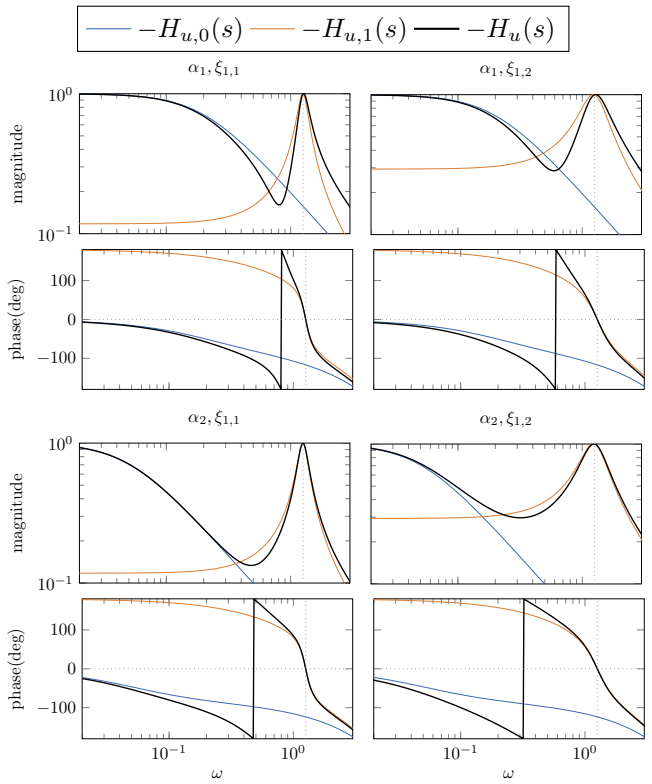

Figure 3: Bode diagrams from d to $\hat{d}$ in the numerical example

Table 2: Performance indicators depending on the observer tuning

	$\alpha_1, \xi_{1,1}$	$\alpha_1, \xi_{1,2}$	$\alpha_2, \xi_{1,1}$	$\alpha_2, \xi_{1,2}$
Settling time (step)	24.2	21.5	79.1	78.4
IAE (step)	6.21	7.16	19.3	22.9
Settling time (sine)	24.3	10	24.5	10.1
IAE (sine)	6.1	2.9	5.77	3.11
Noise amplification	0.33	0.52	0.18	0.37
Sensitivity peak incr.	1.17	1.29	1.13	1.29

coincide also with the lowest deterioration of closed loop robustness (the worsening is at most of 13% with $\alpha_2, \xi_{1,1}$), while the best results in settling time or IAE lead to a higher sensitivity peak (i.e., worse robustness), as it is increased in the order of 29 % (cases $\alpha_1, \xi_{1,2}$ and $\alpha_2, \xi_{1,2}$)

7.1. Control applications of the observer

Figure 6 shows the application of a control system to attenuate the effect of disturbances following the strategies explained in Section 5. We have tested the system under low frequency disturbances, being a unitary ramp (shown in the top plots) and a unitary sinusoidal signal of frequency $\omega_1 = 1.2566$ rad/s (shown in the lower plots). First, we show in the left the response of the system when a pure feed-forward strategy is applied (pure FF, see (39)). We show the ability of the proposal to mitigate sinusoidal signals, and the ability to attenuate the effect of ramp-like disturbances. In the case of ramp disturbances the achieved steady state error is given by (40), whose values

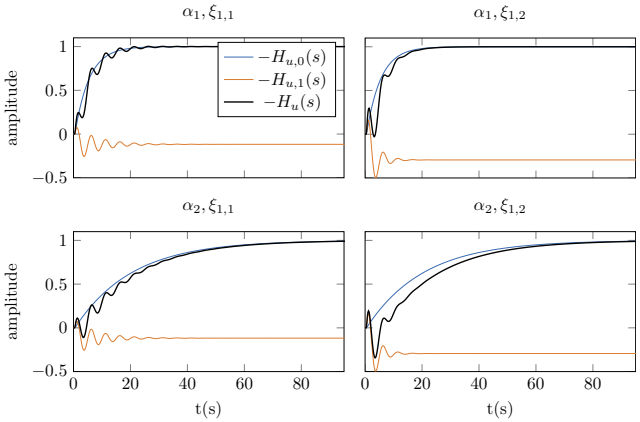

Figure 4: Estimator step disturbance response for the numerical example

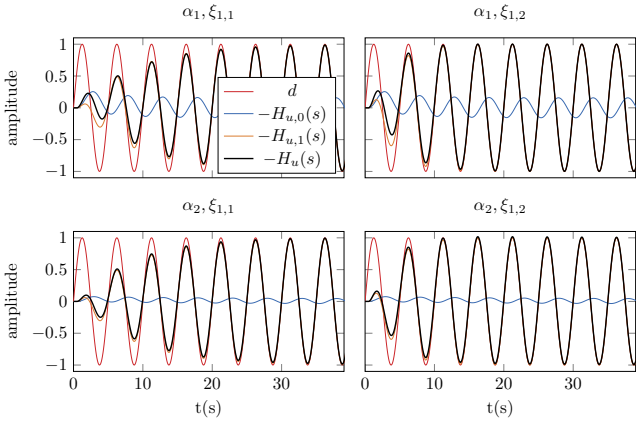

Figure 5: Estimator sine disturbance response

are shown in Table (3) and fit those obtained in the simulation. In the right part we show the use of the disturbance observer together with a PI controller

$$C(s) = K_p + \frac{K_i}{s},$$

leading to a disturbance observer control strategy (DOB, see (41)). The controller is a PI controller designed to guarantee a sensitivity peak $\|S_0(s)\|_\infty = 1.2$ in (45) while maximizing the integral gain K_i, leading to

$$C(s) = 0.377 + \frac{0.42}{s}.$$

The sensitivity peak of the closed loop system is increased when used with the disturbance observer, as shown in Table 3. We see in Figure 6 that the DOB strategy is able to mitigate the effect of ramp disturbances (as a benefit w.r.t. a simple PI control scheme). We see that the use of α_1 leads to better results than α_2 when mitigating the ramp disturbance both in pure FF and DOB. On the other hand, we also see that sinusoidal disturbances can be eliminated when using the disturbance observer, both in pure FF and in DOB. We see that the use of $\xi_{1,2}$ leads to better

Table 3: Performance indicators in control applications

	$\alpha_1, \xi_{1,1}$	$\alpha_1, \xi_{1,2}$	$\alpha_2, \xi_{1,1}$	$\alpha_2, \xi_{1,2}$
SS error (ramp, FF)	6.15	7.11	22.9	26.5
IAE (sine, FF)	19.6	10.7	18.9	11.8
$\|S(s)\|_\infty$	1.38	1.47	1.30	1.40
IAE (ramp, DOB)	73.3	84.9	267.3	309.3
IAE (sine, DOB)	23.0	11.6	21.8	11.1

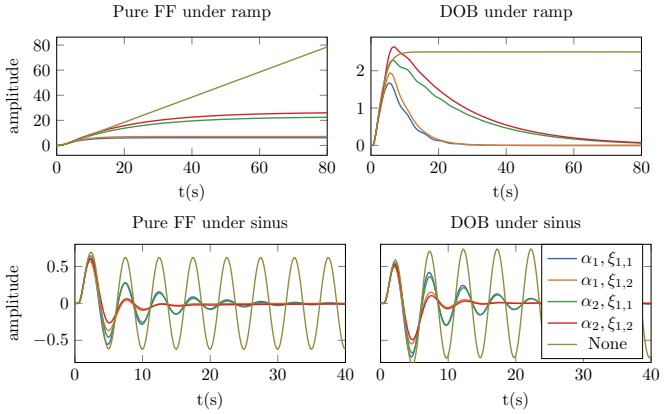

Figure 6: Disturbance rejection: output response of the system when disturbance estimation is used as a control signal to avoid the effect of the disturbance on the controlled output. Pure FF and DOB under ramp and sinusoidal signals is shown.

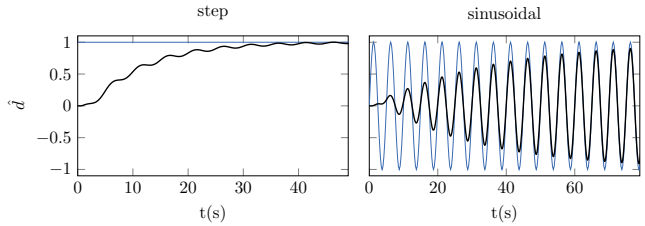

Figure 7: Estimator response with the state space approach

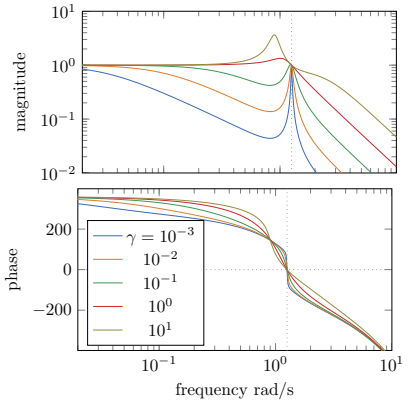

Figure 8: Bode diagram of $G(s)H_y(s)$ of the state space approach

results than $\xi_{1,1}$ when facing sinusoidal disturbances. In all, the combination α_1 and $\xi_{1,2}$ leads to better transient and steady state results in any case at the cost of a higher noise amplification and a slight sensitivity peak increase.

7.2. Comparison with other methods

To compare the approach with a state space one designed through liner quadratic estimator, we first approximate the delay with Pade and obtain the state space representation defined by

$$A = \begin{bmatrix} -5 & 2 \\ 2 & 0 \end{bmatrix}, \; B = \begin{bmatrix} 2 \\ 0 \end{bmatrix}, \; C = \begin{bmatrix} -0.5 & 1 \end{bmatrix}$$

and define disturbance generation matrices

$$A_z = \begin{bmatrix} 0 & 0 & 0 \\ 0 & 0 & 1 \\ 0 & -\left(\frac{2\pi}{5}\right)^2 & 0 \end{bmatrix}, \; C_z = \begin{bmatrix} 1 & 1 & 0 \end{bmatrix}.$$

With this, if we set $\gamma = 10^{-2}$ we obtain the gain $L = [-0.0063,\ 0.1505,\ 0.1000,\ 0.0104,\ -0.1250]^T$ and the response under step and sinusoidal disturbances shown in figure 7. Figure 8 shows the diagram Bode of $H_y(s)G(s)$, i.e., the disturbance tracking ability for γ=10^{-3}, 10^{-2}, 10^{-1}, 10^{0}, 10^{1}. Furthermore, figure9 shows the resulting estimated settling time t_s as a function of γ together with the resulting H_∞ norm of $H_u(s) + H_y(s)G(s)$, that evaluates the control action coupling due to the delay approximation, where we can observe a trade-off between tracking speed and decoupling ability. The settling time has been estimated as $t_s = -(1.4{+}2.53\,(1)^{0.8})/\lambda_{\max} = -3.93/\lambda_{\max}$, being $\lambda_{\max}$ the maximum real part of the eigenvalues of $(\bar{A} - L\,\bar{C})$, by assuming a pair of complex dominant poles, and using expression (30).

As a difference with the proposed approach, with the state space approach we cannot easily modify a given desired frequency range while keeping the frequency response at other ranges. On the other hand, we see that with the state space approach, the input decoupling performance deteriorates if a fast response is required, due to the delay approximation. Furthermore, we cannot assure that the magnitude at the desired frequency is a local maximum as we achieve with our approach.

8. Case study

We have tested the multi-resonant disturbance observer proposed in this work in a chemical industry distillation column, which is depicted in figure 10 . Specifically, this distillation column allows the separation of a 10t/h stream containing around 70% of cyclohexanone (ONE) and 30% of cyclohexanol (OL), both components obtained from cyclohexane oxidation. ONE is used in downstream processes to obtain caprolactam, which is lately used to produce nylon (case study and plant dataset were provided by *UBE Corporation Europe*).

8.1. Process description

Distillation process in this case study works as follows. A mixture stream (ONE and OL) is fed to the column T-3.

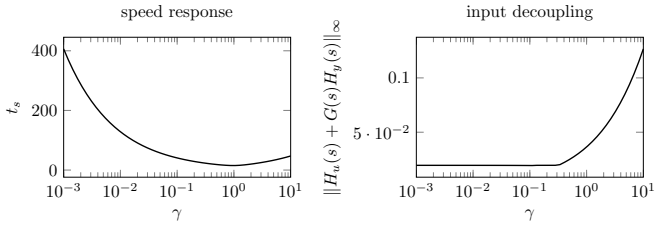

Figure 9: Time and decoupling characteristics as a function of γ

Figure 10: ONE/OL distillation column (the one in the middle of five)

Through the re-boiler E-9, which uses water steam as the heating source, product in the column is heated and then evaporated. These vapours ascend along the column and then they are condensed in a condenser train E-7, composed by a series of heat exchangers that use vented air, cooling water, and brine in various stages. The condensed stream, which contains the product with lower evaporation temperature (in our case, ONE), is collected in the tank D-4, usually named accumulator. Part of this product is fed back to the column T-3. This stream, called reflux, enhances product separation so that if reflux is increased, the effect is that both top product (called distillate) and bottom product become purer; the amount of product with higher evaporation temperature (in our case, OL) in the distillate flow is reduced, as well as the amount of product with lower evaporation temperature (in our case, ONE) in the column bottom flow. The rest of the accumulator product is extracted as the final top product, called distillate. On the other hand, the liquid product in the bottom of the column, which contains the product with higher evaporation temperature (in our case, OL), is extracted through a bottom pipeline.

In this process, top product must have a maximum OL composition of 500ppm, being a high purity product. However, this composition is hard to measure online. In fact, the composition is known through several chemical analysis that can take around 3 hours to give a composition measurement. Due to this, only one measurement every 8 hours is taken in the real plant. One indirect measurement of this composition for a given pressure is the temperature in the column, that can be easily measured online, and whose value is related to the resulting composition. In this particular column we have that a variation of 1^oC corresponds, approximately, with a variation of 100 ppm in the OL composition. Therefore, even small variations of temperatures in the column have a great impact in product composition.

The maximum OL composition is an important constraint because this OL will generate by-products in the downstream caprolactam production process, leading to a final product out of specification. Bottom product usually has an amount of ONE around 5%. Although having ONE in the bottom product is not critical for further processes, it will have an impact on global process efficiency, since this ONE in the bottom product is recovered downstream and fed back to the distillation column at hand. Therefore, to evaporate again the fed back ONE, we should spend more energy, i.e., more steam in the re-boiler.

Considering previous premises, composition of the distillate flow is considered critical and then must be controlled tightly, while composition of the bottom flow is not as critical in terms of product quality but affects production efficiency.

In fact, the ambient temperature causes oscillations in the column temperature in the order of 1^oC (peak-to-peak value), leading to OL composition oscillations in the order of 100 ppm, resulting in a poor quality final product if no compensating action is taken. In this case study we develop our disturbance observer and quantify the potential reduction of the OL composition oscillations if control strategies in section 5 are applied.

8.2. Control scheme

The control scheme, which is implemented in the plant Distributed Control System (DCS), is depicted in figure 11. The column has four control valves, considering the feed is determined by an upstream unit and therefore it is given. All the level and flow controllers represented in the figure are standard PID controllers.

The two main control loops for mass balancing the column are the level controls: one in the accumulator ($LC12$) and the other in the column bottom ($LC10$). The latter is controlled with the bottom control valve, as usually in most distillation columns. The accumulator level can be

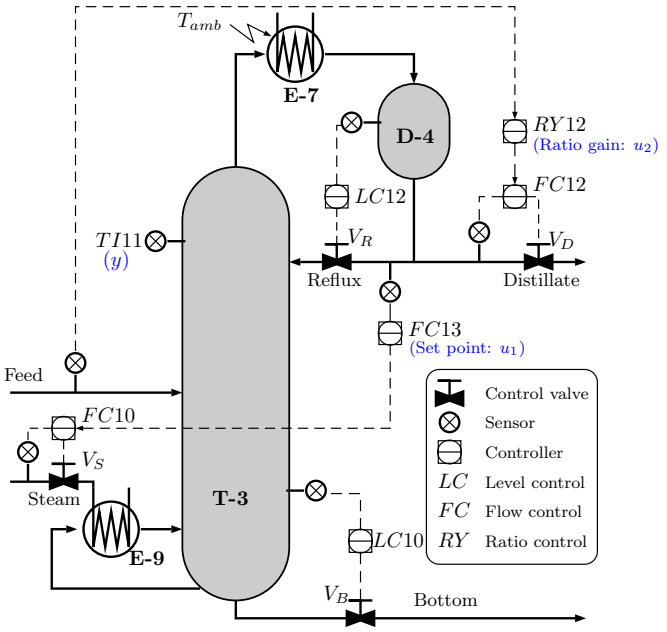

Figure 11: ONE/OL distillation column control scheme

controlled with any of the D-4 outlet valves: reflux or distillate. If it is controlled with the reflux valve, the control scheme is called DV configuration (if bottom level control is handled by the bottom valve), while if the accumulator level were handled by the distillate valve, that would be a LV configuration [48].

Choosing between DV and LV configuration has several implications regarding the column dynamics and disturbance rejection [49, 50]. In a DV configuration, reflux flow is expected to vary due to external disturbances (such as disturbances in the condenser train E-7 or pressure drops in the steam supply), while distillate flow is expected to remain steadier. Therefore, disturbances may affect the separation achieved in the column T-3. On the other hand, in a LV configuration, reflux is expected to be steadier while distillate flow will vary, which can affect a downstream process that receives this stream.

In our case study, the distillation column is controlled in a slight variation of a typical DV configuration.

- The bottom level in column T-3 is controlled by $LC10$, that uses the level measurement and a given setpoint (not shown in the figure) to decide how to manipulate the bottom flow valve V_B.
- The level in accumulator D-4 is controlled by $LC12$, that uses the level measurement and a setpoint (not shown in the figure) to manipulate the reflux valve V_R.
- The distillate flow is controlled by controller $FC12$, that uses the flow measurement and the flow setpoint (that is given by controller $RY12$) to manipulate the distillate valve V_D
- The setpoint of the distillate flow controller $FC12$ is set through a distillate to feed ratio ($RY12$). The ratio gain u_2 is decided by the plant operator regarding the laboratory sample analysis of distillate and bottom compositions, performed every 8 hours and once a day, respectively.
- The steam flow entering re-boiler E-9 is controlled by $FC10$, that uses the steam flow measurement and the setpoint that is given by controller $FC13$ to decide how to manipulate the steam valve V_S.
- The reflux flow entering in the top of the column is controlled by $FC13$. This controller uses the measurement of the reflux flow and a given setpoint u_1 fixed by the operator, and it decides the setpoint value in controller $FC10$. Note that $FC10$ is the slave and $FC13$ the master controller in a cascade configuration. The change in steam flow affects the inlet flow of tank D4, and level controller LC12 controls the reflux flow to match the D4 inlet flow and maintain level. Therefore, a change in steam flow setpoint results in a change in reflux flow, what makes controller $FC13$ feasible.
- Top pressure is not regulated by any controller in this column since the condenser train runs permanently at its maximum capacity, but there are mechanisms like manual valves, which ensure that it is set between acceptable operating limits.

This control scheme has some advantages that makes it suitable for this column context:

- Due to the distillate to feed ratio control ($RY12$), variations in the feed stream (which are quite common since it comes from the bottom flow of another upstream distillation column) are not affecting the mass balance of the column in terms of distillate to bottom ratio, whose variation would have strong effects in top product composition (because it is a high purity product).
- Due to the cascade control of reflux flow ($FC13$) and steam flow control ($FC10$), we can expect that pressure drop disturbances in the steam supply will be rejected by the steam flow controller $FC10$ and, therefore, they will not affect the reflux flow ($FC13$). Disturbances in the condenser train E-7 rebounding in reflux flow must be rejected by the reflux flow controller ($FC13$).

As we have started to mention before, main disturbances in this distillation column are feed variation, steam supply pressure drops and condenser train E-7 disturbances. Feed variation effect is handled by the ratio control ($RY12$). Steam pressure drops are handled by the steam flow control loop ($FC10$) in cascade configuration. Nevertheless, condenser train E-7 disturbances, since it runs always at

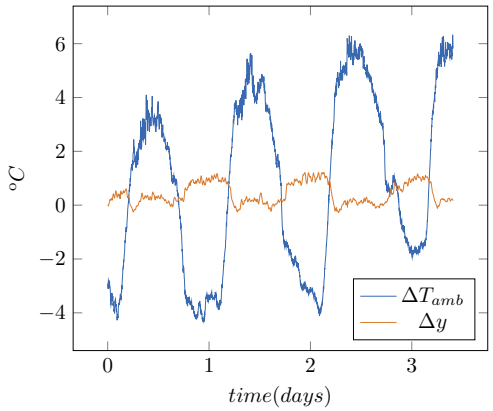

Figure 12: Ambient temperature effect on y

maximum capacity and no pressure regulation in the column is available,must be rejected by the reflux flow controller ($FC13$), which is a slow control loop due to the also slow distillation column dynamics. The condenser train E-7, as mentioned before, is composed of a series of heat exchangers. The first set of exchangers is based in air convection, with six big fans boosting ambient air through the tubes where the evaporated product flows. The second set are heat exchangers using cooling water, which is water in a closed circuit, cooled in refrigeration towers. The third and last set of condensers use brine. First and second set of condensers are very dependent on climate conditions and ambient temperature. Therefore, ambient temperature is a major disturbance for the distillation column, and it must be rejected by the reflux flow PID controller ($FC13$), which is not a fast controller.

8.3. Model identification

As explained before, distillate composition is the main control target of the column. Since it is not directly measured, we find a good indicator of this composition in one of the column temperature sensors that is sensitive to the distillate composition, $TI11$. We consider this temperature as our process output, y. Figure 12 shows a period of several days, where the effect of ambient temperature in the output can be appreciated.

We consider the system model

$$y(s) = G_1(s)(u_1(s) + d(s)) + G_2(s)u_2(s) \tag{54}$$

where d is the input disturbance to be estimated. If we want to relate this disturbance with the ambient temperature, we can model the system as

$$y(s) = G_y(s)\ (G_u(s)\,u(s) + G_T(s)\,\Delta T_{amb}(s))$$

where

$$d(s) = \frac{G_y(s)\,G_T(s)}{G_1(s)}\,\Delta T_{amb}(s)$$

being $G_y(s)$ and $G_T(s)$ unknown transfer functions that cannot be identified with the measurable signals.

The two control actions, which are the set points of the base layer control loops, consist of the reflux ($FC13$) set-point, u_1, and the distillate to feed ratio ($RY12$) gain, u_2. Our objective is to develop an observer of the main disturbance, i.e., the ambient temperature effect on the distillate composition, considered as an input disturbance in the same channel as u_1, named d.

The models of G_1 and G_2, which are $G_{1,m}$ and $G_{2,m}$ respectively, were identified from plant tests where u_1 and u_2 were excited independently while the other input remained constant. Figures 14 and 15 show the identification test.

Figure 13 shows the block diagram of the multi-resonant observer in this application, considering the system model.

As a result of the identification, we obtained

$$\begin{aligned} G_{1,m}(s) &= \left.\frac{\Delta y(s)}{\Delta u_1(s)}\right|_{u_1=1000} = \frac{0.00115(1+286s)}{1+149.5s+5586s^2}e^{-10s}, \\ G_{2,m}(s) &= \left.\frac{\Delta y(s)}{\Delta u_2(s)}\right|_{u_2=0.7} = \frac{48.3}{1+135.4s}, \end{aligned} \tag{55}$$

where time is expressed in minutes, y in ^oC, u_1 in kg/h and u_2 is non-dimensional in the range $[0, 1]$. Based on the model G_1, the multiplicity of the filters is $n_F = 1$.

8.4. Disturbance observer design

Here we discuss the procedure followed for the multi-resonant disturbance observer design (what we refer as MRF for the multi-resonant terms and the low pass filter term), i.e., the selection of the number of resonant terms, and the tuning of the parameters α and the corresponding ξ_i. As we stated before, the best number of resonant terms to include depend on the number of harmonics in the disturbance signal. Also, if we follow the proposed tuning procedure consisting in settling the amount of total noise amplification, we need to decide how to distribute it among the different terms.

For this case study we have compared the following two tuning strategies:

- Equitable noise weighting, i.e., same noise amplification for each term of the MRF observer, according to (37).
- Optimal weighting according to the sampled data.

For the optimal weighting, we have minimized along the dataset the cumulative absolute output error, defined by

$$\int |\tilde{y}(t)|dt = \int |y(t) - \hat{y}(t)|dt, \tag{56}$$

being $\hat{y}$ the estimated output using the models and the estimated disturbance, i.e.

$$\hat{y}(s) = G_{1,m}(s)(u_1(s) + \hat{d}(s)) + G_{2,m}(s)u_2(s). \tag{57}$$

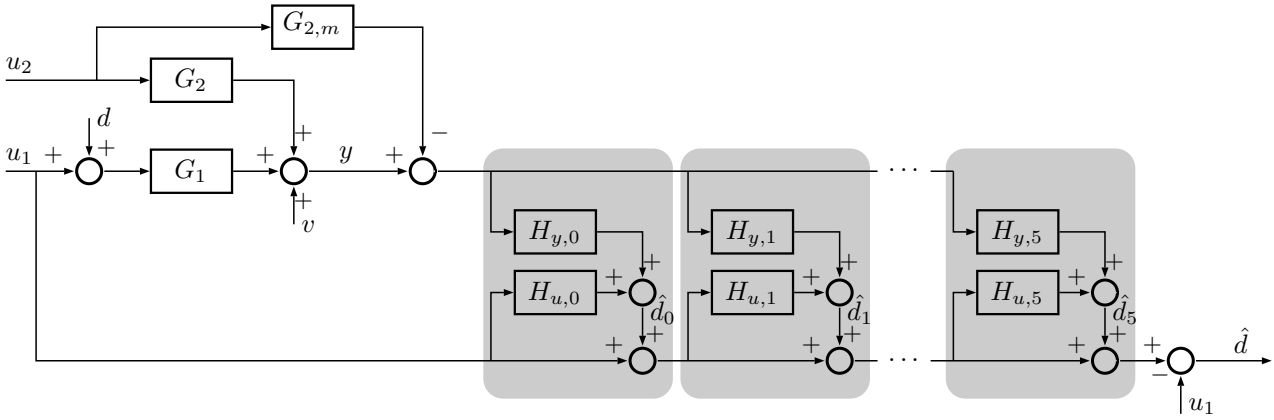

Figure 13: Block diagram of the proposed additive-cascade structure for the experimental case in a sequential interpretation.

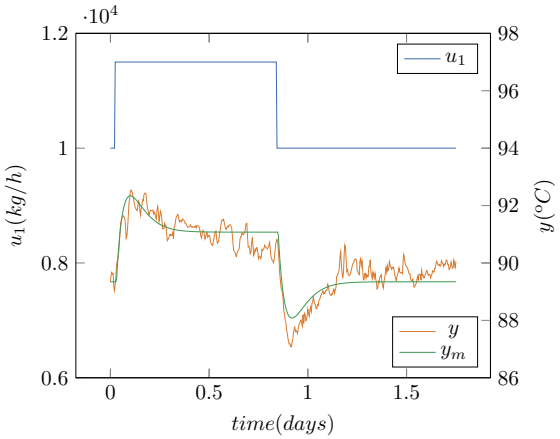

Figure 14: Step test for $G_{1,m}$ identification

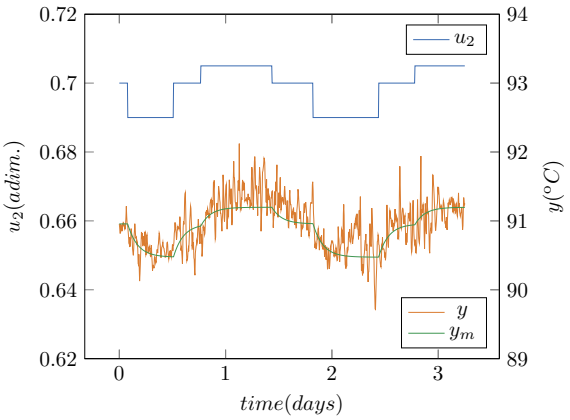

Figure 15: Step test for $G_{2,m}$ identification

In both strategies we have set a total noise amplification of 300 according to (36), and we have done simulations for different number of resonant terms n_ω. Given that the measurement noise amplitude is most of the time in the order of 0.1^oC, this means that the noisy part of $\hat{d}$ will have an amplitude in the order of $30kg/h$, and, considering that the expected values for $\hat{d}$ are in the order of magnitude of u_1 (from 0 to $1.2 \cdot 10^4$ kg/h) this means only a 0.25% for the total range of u_1. After applying our technique, $\hat{d}$ has resulted to be in the range from 0 to 1000 and thus, the amplitude in $\hat{d}$ due to noise is in the order of 3% w.r.t. its range (see Figure 21).

Due to the daily periodicity of the disturbance, we set the frequency of the resonant terms for a corresponding period of 24 hours and their consequent harmonics. To make it more intuitive, the performance result in each case is given in terms of the Average Absolute Error (AAE) of the output estimation in consonance with (56) and (57), which is in units of ^oC. Figure 16 shows these results. If no disturbance observer is included, i.e., $\hat{d} = 0$ in (57), $AAE = 0.455^oC$. This result is useful to give insight about the contribution of the disturbance observer (best case in figure 16 achieves $AAE = 0.106^oC$, which means a 75% reduction of the average absolute estimation error w.r.t. the case where $\hat{d} = 0$).

Supported by these results, we decide to set the number of resonant terms to $n_\omega = 5$. To evaluate the performance of the proposed MRF, in the next section we compare it with an observer that only has the low-pass filter, without any resonant terms, which we refer to as LPF observer. For the tuning of the parameter α of the LPF observer, we set the same noise amplification as for the MRF observer, according to (36). The tuning parameters obtained for the LPF observer and the MRF with both tuning strategies are presented in table 4.

As stated in the section of control application of the disturbance observer, one possible use of this estimate $\hat{d}$ is to modify input u_1 as $u_1 - \hat{d}$ in order to mitigate the effect of the ambient temperature over temperature y. Unfortunately it has not been possible to test this strategy in the real plant. However, with the theoretical development, we can predict that the variations of the temperature y, that are in the order of 1 degree in absolute value, would be reduced to a value equal to the one obtained in the reconstruction error $\tilde{y}$ shown in the figures, that is in the order of 0.3 degrees. This could mean an approximate reduction

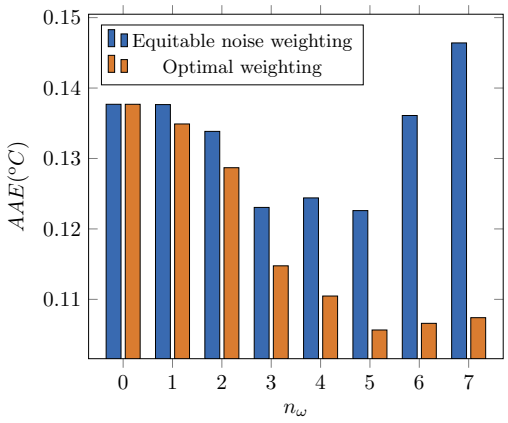

Figure 16: Performance of tuning strategies for several values of n_ω

Table 4: Observers tuning

Observer	Parameter	$t_s(min)$	Noise ampl.
LPF	$\alpha = 56.4$	232	300
MRF	$\alpha = 339.6$	1345	50
(Eq.)	$\xi_1 = 0.338$	2675	50
	$\xi_2 = 0.17$	2659	50
	$\xi_3 = 0.113$	2667	50
	$\xi_4 = 0.086$	2628	50
	$\xi_5 = 0.069$	2621	50
MRF	$\alpha = 126.7$	508	134
(Opt.)	$\xi_1 = 0.492$	1841	72.8
	$\xi_2 = 0.088$	5127	26
	$\xi_3 = 0.077$	3909	34
	$\xi_4 = 0.021$	10730	12.3
	$\xi_5 = 0.030$	6014	21.7

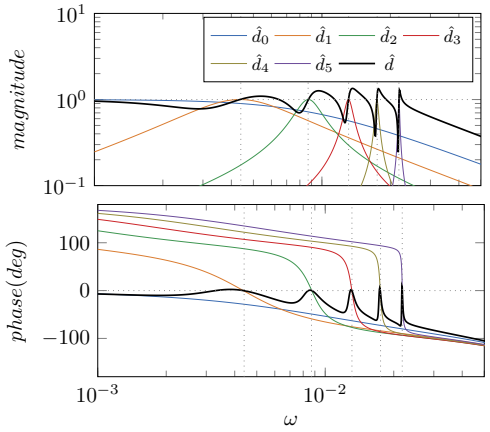

Figure 17: Bode diagram from d to $\hat{d}$.

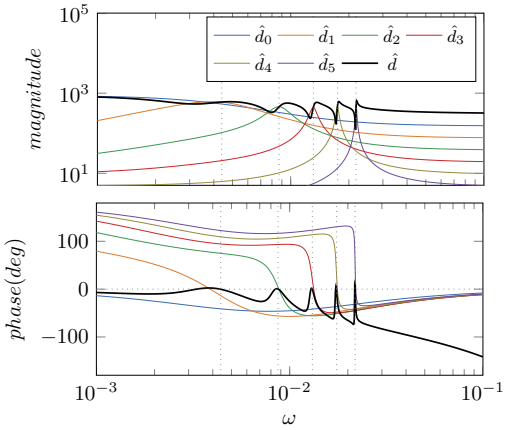

Figure 18: Bode diagram from v to $\hat{d}$

of 70 ppm in the composition fluctuation due to the disturbances (according to the approximate relation between temperature and composition changes), if a feed-forward control scheme as stated in section 5.1 is implemented.

For the MRF observer tuned with optimal weighting, figure 17 shows the Bode diagram from d to $\hat{d}$ for each term of the observer. We can check how, for the targeted frequencies, the magnitude is equal to 1 and the phase is equal to 0º at $\omega = \omega_i, \forall i \in \{1, ..., 5\}$. Figure 18 shows the Bode diagram from noise signal v to disturbance estimation $\hat{d}$. We see how the noise effect on the MRF observer adds up the noise effect of each of the terms.

8.5. Results

Since disturbance d is not measured, and therefore it is impossible to compare with the disturbance estimation $\hat{d}$, to illustrate the goodness of the obtained results we have reconstructed an output estimation $\hat{y}$ from the inputs u_1 and u_2 and the disturbance estimation $\hat{d}$, considering the input-output models available according to (56) and (57), and then we have compared it with the real output y.

Figure 19 compares the real output y (as its increment from the beginning of the sampled data) with the prediction obtained with both the LPF and the MRF filter. In figure 20, we can see the output error $\tilde{y}$ for both observers. We also show in the figure the difference between the output error obtained with the LFP and the MRF observer, to see how a smaller error is obtained with the MRF. The MRF achieves a better performance especially in the areas where y presents more abrupt changes.

Figure 21 shows the disturbance estimation in both LPF and MRF cases. Again, we appreciate a faster estimation over disturbance changes in the case of the MRF observer. Finally, in figure 22 we can evaluate the individual response of each observer included in the MRF observer, according to the sequential interpretation mentioned in section 3.5 (see figure 13).

9. Prospect for practitioners

As we have seen in the numerical example and case study section, the techniques explained in this work are suitable to improve the performance of industrial processes if the next conditions are fulfilled:

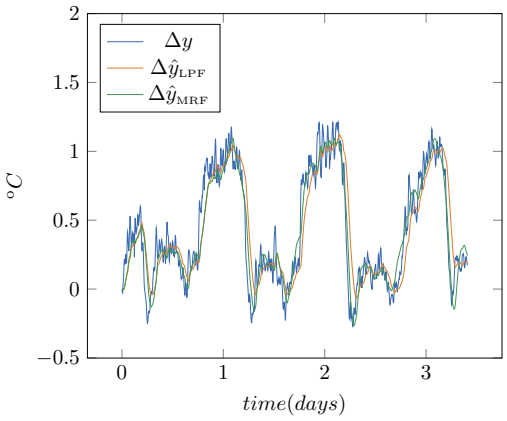

Figure 19: Output estimation with LPF and MRF observers.

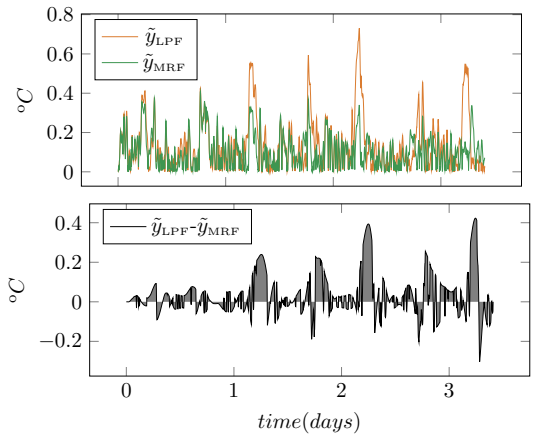

Figure 20: Output estimation error with LPF and MRF observers.

- The process faces oscillatory disturbances that have a main frequency in the order of the dynamics of the open loop process, or higher.
- The disturbance cannot be measured, or if its dynamics effect on the output cannot be identified.
- The effect of the disturbances is significant and cannot be rejected with standard feedback control.

If previous conditions are met, we can develop an observer following section 4.2, and implement a pure feed-forward scheme (see section 5.1) or in combination with a feedback controller (see section 5.2). This can be summarized as follows:

1. Gather a data set $\mathcal{X}$ with enough excitation in signal $u(t)$ to identify a model of the process $G(s)$.
2. Gather a data set $\mathcal{Y}$ long enough to show the effect of oscillatory disturbances on output $y(t)$.
3. Design an observer according the rules in section 4.2, leading to $H_u(s)$ and $H_y(s)$ in (13) and (14) whose terms $H_{u,i}(s)$ and $H_{y,i}(s)$ are detailed in (21), (22), (24) and (25).

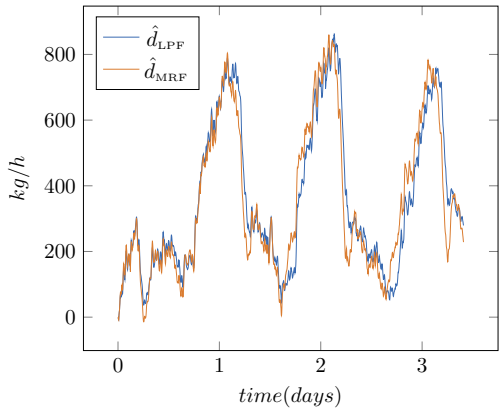

Figure 21: Disturbance estimation with LPF and MRF observers.

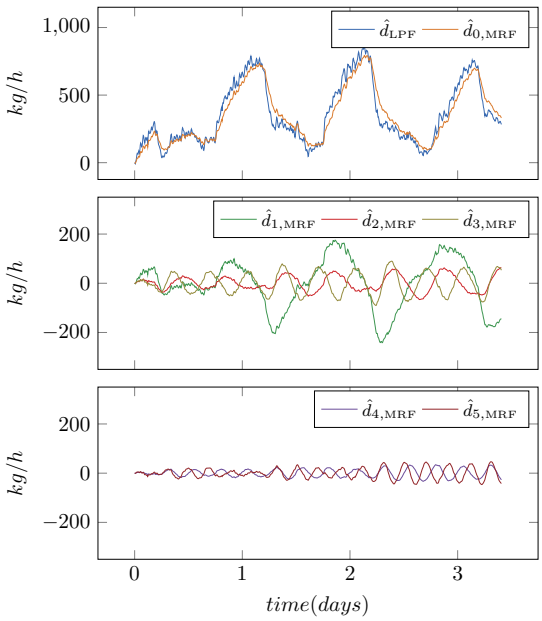

Figure 22: Disturbance estimation components of LPF and MRF observers.

4. Implement a control scheme including the observer either as a pure feed forward control (see (39)), or together with a standard feedback controller (see (41)). In this last case, the effect on the closed-loop robustness must be considered as quantified in (46) for the design of both the controller and the observer.

10. Conclusions

In this work we have proposed a multi-resonant disturbance observer to estimate periodic disturbances, and its application to periodic ambient temperature disturbances in an industrial distillation column. The structure of the proposed observer is a cascade additive-multiplicative scalable one, based on simple transfer functions, that allows the easy implementation in industrial control systems. It allows the user to easily include the desired terms to estimate not only the low frequency component but also the

required periodic components of the disturbance. Furthermore, the proposal allows the user to easily add new resonant terms for the estimation of new frequency components, without affecting the previous ones.

The number of tuning parameters is small, and a uncomplicated design strategy is proposed to tune those parameters, based on straightforward relationships between those parameters and some physically meaningful performance indices, as settling times or high frequency measurement noise amplification.

The estimated disturbance signal can be directly used in an open loop feed forward scheme, that is the situation of the real case study. In that case the improvement of disturbance rejection is evident. The estimated disturbance can also be used in a feed-forward closed loop scheme. In that case it affects the closed-loop robustness, and we show how to quantify this effect to take it into account in the disturbance observer design.

We present a numerical example to clarify the proposed observer structure and the effect of the tuning parameters. Finally, we study a real case for a distillation column that operates in a chemical plant. We estimate a periodic disturbance caused by ambient temperature, showing the results according to several tuning strategies and comparing them with the estimation results obtained with an observer that only has a low-pass filter, without any resonant terms. With that, we conclude that the multi-resonant disturbance observer presents a better performance in this case study. The real plant implements an open loop scheme and the implementation of the open loop feed forward strategy with the estimated disturbance is expected to reduce the fluctuation of the column temperature in around 0.7 degrees (equivalent to 70 ppm en distillate composition).

Acknowledgements

The authors want to thank *UBE Corporation Europe* for providing the case study and the historical data used for the disturbance observer test.

Appendix A. Product demonstration

In this appendix we demonstrate that given a sequence $\{x_0, x_1, \ldots, x_n\}$, the following equivalence holds

$$-\sum_{i=0}^{n} x_i \prod_{j=i+1}^{n} (1+x_i) = 1 - \prod_{i=0}^{n}(1+x_i). \tag{A.1}$$

Let us first expand the expression $\prod_{i=0}^{n}(1+x_i)$

$$\begin{aligned}
&\prod_{i=0}^{n}(1+x_i) = (1+x_0)\prod_{i=1}^{n}(1+x_i) \\
&= x_0\prod_{i=1}^{n}(1+x_i) + \prod_{i=1}^{n}(1+x_i) \\
&= x_0\prod_{i=1}^{n}(1+x_i) + x_1\prod_{i=2}^{n}(1+x_i) + \prod_{i=2}^{n}(1+x_i) \\
&= x_0\prod_{i=1}^{n}(1+x_i) + x_1\prod_{i=2}^{n}(1+x_i) \\
&+ x_2\prod_{i=3}^{n}(1+x_i) + \cdots + x_{n-1}(1+x_n) + (1+x_n).
\end{aligned} \tag{A.2}$$

We see then that we can state the following equality

$$\prod_{i=0}^{n}(1+x_i) = 1 + \sum_{i=0}^{n} x_i \prod_{j=i+1}^{n}(1+x_i), \tag{A.3}$$

that, reordering, leads to (A.1).

Appendix B. Other performance indices

Some indicators that explain the transient behaviour can be obtained with tractable expressions as

- Cumulative error under a step in d if only the low pass term was present (with no resonant terms):

$$\lim_{t\to\infty}\int_0^t \tilde{d}(t)dt = n_F\alpha + \sum \delta_i + T. \tag{B.1}$$

- Cumulative error for sinusoidal d of frequency ω_i if only the oscillatory term for ω_i was present:

$$\lim_{t\to\infty}\int_0^t \tilde{d}(t)dt = \frac{1}{\omega_i}\left(1 - \frac{(2\xi_i \sin(\phi_i))^{n_F}}{|G_N(j\omega_i)|}\right). \tag{B.2}$$

- Cumulative squared error for each of the terms for its design frequency under the assumption of $G_N(s) = 1$ and $n_F = 1$. In the case of the low pass filter term, it leads to

$$\lim_{t\to\infty}\int_0^t \tilde{d}(t)^2dt = \frac{\alpha}{2},$$

and, for the oscillatory terms

$$\lim_{t\to\infty}\int_0^t \tilde{d}(t)^2dt = \frac{1}{4\xi_i\omega_i}.$$

This can be obtained computing, respectively the H_2 norm of the systems

$$\left(1 - \frac{1}{1+\alpha\, s}\right)\frac{1}{s}, \quad \left(1 - \frac{2\xi_i\omega_i s}{s^2 + 2\xi_i\omega_i s + \omega^2}\right)\frac{\omega}{s^2+\omega^2}.$$

However, one must take care with the expression for the cumulative error for the resonant terms of the estimator (B.2). Due to the oscillatory nature of these terms, and the sign variation of the signal, that index is not a representative metric for the goodness of the estimator. For instance, if the cumulative error is zero, that implies that the signal has the same error in positive terms as in negative along time. On the other hand, the H_2 norm has complex expressions for systems presenting non-invertible dynamics ($G_N(s) \neq 1$) or that lead to $n_F > 1$. Thus, the proposal is to use the approximated settling time expressions derived from the poles as they have easy to understand physical meanings, and are in comparable magnitude for both low pass filter and resonant terms.

Appendix C. Settling time approximation

In this section we show the steps followed to obtain the expression (30) for settling time approximation. First, we define the settling time (t_s) as the time elapsed from input change to the time needed to reach a value that is within 98% and 1.02% of the final value. In figure C.23 we show the time response for transfer function

$$G(s) = \frac{1}{(1 + 1\,s)^n}$$

under unitary step input for different values of n in the set $\{1, 2, \ldots, 7\}$. We include a mark '·' to indicate the measured settling time when crossing that 98% band. Then, in figure C.24 we show the measured settling times for each n in circles and, for comparison purposes, we also include with symbol $\times$ the value predicted by the proposed expression

$$t_s \approx 1.4 + 2.53\, n^{0.8}, \tag{C.1}$$

showing the goodness of the approximation. As the times are scalable in the aforementioned transfer function, the general expression to approximate the settling time in a function as

$$G(s) = \frac{1}{(1 + \alpha s)^n}$$

is

$$t_s \approx (1.4 + 2.53\, n^{0.8})\, \alpha. \tag{C.2}$$

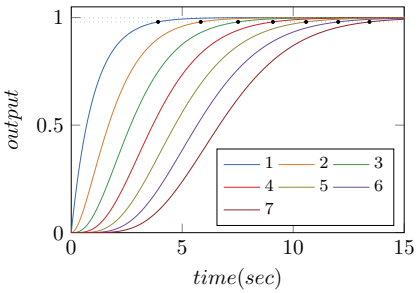

Figure C.23: Step response of $G(s) = \frac{1}{(1+s)^n}$ for different values of n.

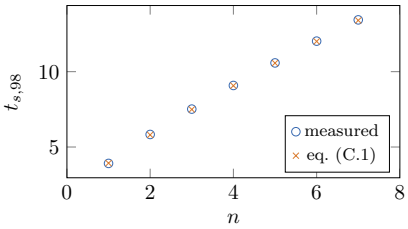

Figure C.24: Settling time of $G(s) = \frac{1}{(1+s)^n}$ for different values of n. Comparison between measured values and estimated ones.

References

[1] Z. Gao, On the centrality of disturbance rejection in automatic control, ISA transactions 53 (4) (2014) 850–857.

[2] W.-H. Chen, J. Yang, L. Guo, S. Li, Disturbance-observer-based control and related methods—an overview, IEEE Transactions on industrial electronics 63 (2) (2015) 1083–1095.

[3] J. Chen, R. J. Patton, Robust model-based fault diagnosis for dynamic systems, Vol. 3, Springer Science & Business Media, 2012.

[4] S. X. Ding, Model-based fault diagnosis techniques: design schemes, algorithms, and tools, Springer Science & Business Media, 2008.

[5] D. Tena, I. Peñarrocha-Alós, A simple procedure for fault detectors design in siso systems, Control Engineering Practice 96 (2020) 104302.

[6] J.-H. She, M. Fang, Y. Ohyama, H. Hashimoto, M. Wu, Improving disturbance-rejection performance based on an equivalent-input-disturbance approach, IEEE Transactions on Industrial Electronics 55 (1) (2008) 380–389.

[7] J. Yang, S. Li, X. Chen, Q. Li, Disturbance rejection of dead-time processes using disturbance observer and model predictive control, Chemical engineering research and design 89 (2) (2011) 125–135.

[8] L. Sun, D. Li, K. Y. Lee, Enhanced decentralized pi control for fluidized bed combustor via advanced disturbance observer, Control Engineering Practice 42 (2015) 128–139.

[9] J. G. Kim, C. H. Han, S. K. Jeong, Disturbance observer-based robust control against model uncertainty and disturbance for a variable speed refrigeration system, International Journal of Refrigeration 116 (2020) 49–58.

[10] L. F. A. Pereira, J. V. Flores, G. Bonan, D. F. Coutinho, J. M. G. da Silva, Multiple resonant controllers for uninterruptible power supplies—a systematic robust control design approach, IEEE Transactions on Industrial Electronics 61 (3) (2013) 1528–1538.

[11] G. A. Ramos Fuentes, J. A. Cortés-Romero, Z. Zou, R. Costa-Castelló, K. Zhou, Power active filter control based on a resonant disturbance observer, IET Power Electronics 8 (4) (2015) 554–564.

[12] M. Mellincovsky, V. Yuhimenko, M. M. Peretz, A. Kuperman, Low-frequency dc-link ripple elimination in power converters with reduced capacitance by multiresonant direct voltage regulation, IEEE Transactions on Industrial Electronics 64 (3) (2016) 2015–2023.

[13] M. Elkayam, S. Kolesnik, A. Kuperman, Guidelines to classical frequency-domain disturbance observer redesign for enhanced rejection of periodic uncertainties and disturbances, IEEE Transactions on Power Electronics 34 (4) (2018) 3986–3995.

[14] Z. Song, Z. Zhang, H. Komurcugil, C. H. Lee, Controller-based periodic disturbance mitigation techniques for three-phase two-level voltage-source converters, IEEE Transactions on Industrial Informatics 17 (10) (2021) 6553–6568.

[15] K. Cho, J. Kim, S. B. Choi, S. Oh, A high-precision motion control based on a periodic adaptive disturbance observer in a pmlsm, IEEE/ASME Transactions on Mechatronics 20 (5) (2014) 2158–2171.
[16] S. K. Patel, S. R. Arya, R. Maurya, B. C. Babu, Control scheme for dstatcom based on frequency-adaptive disturbance observer, IEEE Journal of Emerging and Selected Topics in Power Electronics 6 (3) (2018) 1345–1354.
[17] M. Vekić, M. R. Rapaić, T. B. Šekara, S. Grabić, E. Adžić, Multi–resonant observer pll with real-time estimation of grid unbalances, International Journal of Electrical Power & Energy Systems 108 (2019) 52–60.
[18] B. Guo, S. Bacha, M. Alamir, A. Hably, C. Boudinet, Generalized integrator-extended state observer with applications to grid-connected converters in the presence of disturbances, IEEE Transactions on Control Systems Technology 29 (2) (2021) 744–755.
[19] H. Muramatsu, S. Katsura, An adaptive periodic-disturbance observer for periodic-disturbance suppression, IEEE Transactions on Industrial Informatics 14 (10) (2018) 4446–4456.
[20] Y. Hori, A review of torsional vibration control methods and a proposal of disturbance observer-based new techniques, IFAC Proceedings Volumes 29 (1) (1996) 990–995.
[21] S. Katsura, K. Ohnishi, Absolute stabilization of multimass resonant system by phase-lead compensator based on disturbance observer, IEEE Transactions on Industrial Electronics 54 (6) (2007) 3389–3396.
[22] Q. He, X. Wang, Time–frequency manifold correlation matching for periodic fault identification in rotating machines, Journal of Sound and Vibration 332 (10) (2013) 2611–2626.
[23] R. Madonski, M. Stanković, S. Shao, Z. Gao, J. Yang, S. Li, Active disturbance rejection control of torsional plant with unknown frequency harmonic disturbance, Control Engineering Practice 100 (2020) 104413.
[24] H. Coral-Enriquez, J. Cortés-Romero, S. A. Dorado-Rojas, Rejection of varying-frequency periodic load disturbances in wind-turbines through active disturbance rejection-based control, Renewable Energy 141 (2019) 217–235.
[25] E. Sariyildiz, K. Ohnishi, A guide to design disturbance observer, Journal of Dynamic Systems, Measurement, and Control 136 (2) (2014) 021011.
[26] A. Castillo, P. J. García Gil, P. Albertos, Disturbance observer-based controllers: operating principles and design strategies, Revista Iberoamericana de Automática e Informática industrial 19 (4) (2022) 343–355.
[27] H. Muramatsu, Separation and estimation of periodic/aperiodic state, Automatica 140 (2022) 110263.
[28] I. Alsogkier, C. Bohn, Rejection and compensation of periodic disturbance in control systems, The International Journal of Engineering and Information Technology (2017).
[29] P. Shen, H.-X. Li, A multiple periodic disturbance rejection control for process with long dead-time, Journal of Process Control 24 (9) (2014) 1394–1401.
[30] X. Wen, Y. Sun, J. Wang, X. Yao, Rejection of time-varying frequency sinusoidal disturbance using refined observer for a class of uncertain systems, ISA Transactions 100 (2020) 136–144.
[31] J. Cheng, Y. Yang, H. Shao, H. Pan, J. Zheng, J. Cheng, Enhanced periodic mode decomposition and its application to composite fault diagnosis of rolling bearings, ISA Transactions (2021).
[32] M. Fadali, S. Gummuluri, Robust observer-based fault detection for periodic systems, in: Proceedings of the 2001 American Control Conference.(Cat. No. 01CH37148), Vol. 1, IEEE, 2001, pp. 464–469.
[33] P. Zhang, S. X. Ding, G. Wang, D. Zhou, Fault detection of linear discrete-time periodic systems, IEEE Transactions on Automatic Control 50 (2) (2005) 239–244.
[34] R. Yao, H. Jiang, Z. Wu, K. Wang, Periodicity-enhanced sparse representation for rolling bearing incipient fault detection, ISA Transactions 118 (2021) 219–237.
[35] Z. Gao, S. Hu, F. Jiang, A novel motion control design approach based on active disturbance rejection, in: Proceedings of the 40th IEEE conference on decision and control (Cat. No. 01Ch37228), Vol. 5, IEEE, 2001, pp. 4877–4882.
[36] J. Han, From pid to active disturbance rejection control, IEEE transactions on Industrial Electronics 56 (3) (2009) 900–906.
[37] R. Zhou, W. Tan, Analysis and tuning of general linear active disturbance rejection controllers, IEEE Transactions on Industrial Electronics 66 (7) (2018) 5497–5507.
[38] B. Martinez, J. Sanchis, S. Garcia-Nieto, M. Martinez, Active disturbance rejection control: a guide for design and application, Revista Iberoamericana de Automática e Informática industrial 18 (3) (2021) 201–217.
[39] H. Muramatsu, S. Katsura, Design of an infinite-order disturbance observer enhancing disturbance suppression performance, IEEJ Journal of Industry Applications 6 (3) (2017) 192–198.
[40] H. Muramatsu, S. Katsura, An enhanced periodic-disturbance observer for improving aperiodic-disturbance suppression performance, IEEJ Journal of Industry Applications 8 (2) (2019) 177–184.
[41] M. Zheng, X. Lyu, X. Liang, F. Zhang, A generalized design method for learning-based disturbance observer, IEEE/ASME Transactions on Mechatronics 26 (1) (2020) 45–54.
[42] R. Lewis, Modelling control systems using IEC 61499: Applying function blocks to distributed systems, no. 59, IET, 2001.
[43] M. Chaabene, Measurements based dynamic climate observer, Solar Energy 82 (9) (2008) 763–771.
[44] D. Tena, I. Peñarrocha-Alós, R. Sanchis, Performance, robustness and noise amplification trade-offs in disturbance observer control design, European Journal of Control 65 (2022) 100630.
[45] I. Peñarrocha-Alós, E. Sales-Setién, D. Tena, Actuator fault tolerant control proposal for pi controlled siso systems, IFAC-PapersOnLine 51 (24) (2018) 680–687.
[46] G. A. R. Fuentes, J. A. Cortés-Romero, Z. Zou, R. Costa-Castelló, K. Zhou, Power active filter control based on a resonant disturbance observer, IET Power Electronics 8 (4) (2015) 554–564.
[47] E. Sales-Setién, I. Peñarrocha-Alós, Trade-offs on fault estimation via proportional multiple-integral and multiple-resonant observers for discrete-time systems, IET Control Theory & Applications 13 (5) (2019) 659–671.
[48] S. Skogestad, Dynamics and control of distillation columns-a critical survey, in: Dynamics and Control of Chemical Reactors, Distillation Columns and Batch Processes, Elsevier, 1993, pp. 11–35.
[49] S. Skogestad, M. Morari, Understanding the dynamic behavior of distillation columns, Industrial & engineering chemistry research 27 (10) (1988) 1848–1862.
[50] S. Skogestad, The dos and don'ts of distillation column control, Chemical Engineering Research and Design 85 (1) (2007) 13–23.